Mn control in zinc electrowinning process by electrochemical means using Pb-Ag anode

Mémoire

Mohsen Yaghoubi

Maîtrise en génie des matériaux et de la métallurgie - avec mémoire
Maître ès sciences (M. Sc.)

Québec, Canada

Résumé

Les conditions optimales pour l'élimination du dioxyde de manganèse (MnO_2) en utilisant une anode Pb-0.7 pd% d'Ag ont été étudiées en utilisant des électrolytes simulant les conditions pour le fonctionnement de purification et d'extraction électrolytique. L'effet de la densité, de la température, du pH et de la concentration de manganèse sur l'efficacité du courant de formation de MnO_2 et les tensions anodiques ont été étudiés à l'aide d'essais galvanostatiques. La spectroscopie d'émission atomique par plasma micro-ondes (MP-AES) a été utilisée pour mesurer la concentration d'ions manganèse dans les électrolytes.

Des essais de voltamétrie linéaire à balayage (LSV) ont été menés pour étudier l'effet de la température et de la concentrations de Mn^{2+} sur la réaction de dégagement d'oxygène (OER) et la formation de MnO_2. La microscopie électronique à balayage avec spectroscopie à dispersion d'énergie (SEM-EDS), la diffraction des rayons X (XRD) et la fluorescence X (XRF) ont été utilisées pour la caractérisation de surface et les compositions chimiques. Les résultats ont montrés que les conditions d'extraction électrolytiques fonctionnels pour éliminer le MnO_2 consiste à utiliser la Pb-0.7 pd% d'Ag. L'efficacité de courant (CE) la plus élevée de l'élimination du manganèse était de 21 %, ce qui était obtenu dans l'électrolyte à pH 1 et à une densité de courant de 125 A m^{-2} à 40 °C après 2 h d'électrolyse. La valeur d'efficacité a été augmentée à 28 % à l'aide d'anodes neuves remplacées toutes les 30 minutes.

Abstract

The optimum conditions for manganese dioxide (MnO_2) removal using Pb-0.7 wt.% Ag anode have been investigated using electrolytes simulating the purification and electrowinning operating conditions. The effect of current density, temperature, pH and manganese concentration on the current efficiency of MnO_2 formation and anodic voltages have been studied using galvanostatic tests. Microwave plasma atomic emission spectroscopy (MP-AES) has been used to measure the concentration of manganese ions in the electrolytes.

Linear sweep voltammetry (LSV) tests were conducted to study the effect of temperature and Mn^{2+} concentrations on oxygen evolution reaction (OER) and MnO_2 formation. Scanning electron microscopy with energy dispersive spectroscopy (SEM-EDS), X-ray diffraction (XRD) and X-ray fluorescence (XRF) were used to study the surface characterizations and chemical compositions. The results revealed that the operating electrowinning conditions are more appropriate for MnO_2 removal on Pb-0.7 wt.% Ag surface. The highest current efficiency (CE) of manganese removal was 21 % which obtained in the electrowinning electrolyte at pH 1 at 125 A m^{-2} at 40 °C after 2 h of electrolysis. The current efficiency value was increased to 28 % using fresh anodes replaced each 30 minutes.

Table of Contents

List of Tables

List of Figures

Acknowledgments

I would like to express my special thanks of gratitude to my supervisor, professor Houshang D. Alamdari who gave me the golden opportunity to do this wonderful project which also helped me in doing a lot of research and I came to know about so many new things, I am really thankful to him.

I gratefully acknowledge Dr. Fariba Safizadeh for her helpful advices throughout this reasearch. Her advices, direction and encouragements and the valuable assistance was very important and are acknowledged.

I would like to acknowledge my deep sense of gratitude to Georges Houlachi for his support and valuable advices.

I would like to thank the financial support of the National Science and Engineering Research Council (NSERC), CEZin and DeNora is gratefully appreciated.

I wish to thank all the faculty members & staffs of the Mining, Metallurgical and Materials Engineering Department of Université Laval specially, Guillaume Gauvin and Vicky Dodier, for their friendship, support and help during the project.

Last but not the least, I would like to express my gratefulness to my parents and brothers, for their endless support and encouragement.

Introduction

Zinc is an important element for human beings and one of the oldest metals produced. Zinc is a transition metal of atomic number 30, the 23rd most abundant element on earth and the second most abundant transition metal in organisms after iron (Fe) [1]. Zinc is a silvery blue-gray metal and it melts at 419.5 °C. Also, the boiling point of zinc is 907 °C and the density of zinc at 20 °C is 7.14 g cm^{-3}. The naturally occurring zinc has five stable isotopes with average of isotopic compositions of ^{64}Zn, 48.98%; ^{66}Zn, 27.81%; ^{67}Zn, 4.11%; ^{68}Zn, 18.57%; ^{70}Zn, 0.62% [2, 3]. The major application of zinc is for coating of iron and steel, so called galvanized steel, because of its excellent resistance to corrosion in the atmosphere [4]. Table 1 shows the major applications of zinc.

Table 1. The principal world uses of zinc [5].

Applications		**%**	**%**
Zinc coatings – total			37
	Galvanizing-sheet and strip	18	
	Products	11	
	Wire, tube	5	
	Other zinc coatings	3	
Brass			20
Die casting alloys			16
Rolled zinc			10
Zinc oxide			10
Miscellaneous			7

The annual production of zinc is around 10 millions of tons per year, with this amount growing every year [4]. There are many mines around the world and the largest producers are located in Australia, Canada, Peru, the United States, Mexico, Ireland, Russia, Spain, Sweden, North Korea, China and Japan.

In order to obtain the pure zinc metal, a series of purification process including the roasting, leaching, purification and electrowinning are required [6]. These processes are explored in the next chapter. The electrowinning step is the most consumer of energy during the zinc purification process, due to the overpotential of oxygen on the anode[7].

Typically, the lead-based anodes are used for electrowinning process. These type of anodes have a good stability during the zinc electrowinning process, but having the high oxygen evolution overpotential, increase significantly the energy consumption [6, 7]. in order to decrease the energy consumption, there is a possibility of using new types of anodes called mixed metal oxide (MMO) anodes [8].

The MMO anodes could reduce the oxygen evolution overpotential and subsequently increase the energy efficiency [8]. In another hand, presence of manganese ions in the electrolyte could cover the coating MMO anodes during the electrolysis process [9]. Therefore, in order to use of MMO anodes, the concentration of manganese ions must be controlled.

Objectives

The objective of this work is to explore the possibility of removing manganese from zinc electrolyte using lead-based anodes. Manganese is the major obstacle in using new types of anodes in this industry. The new types of anodes are eventually offer substantial energy saving in zinc electrowinning process by reducing the oxygen evolution potential. Table 2 presents various components of cell voltage for an operating plant at 500 A m^{-2} at 38 °C in an electrolyte containing 160 g L^{-1} H_2SO_4 and using lead-0.5 wt.% silver as anode and aluminum as cathode [7]. As shown in this table, it can be clearly observed that the anode electrode potential and oxygen overvoltage are major factors for energy consumption, representing 60 % of the total cell voltage and almost 25 % of total cell voltage just for the oxygen overvoltage.

Table 2. Components of cell voltage [7].

Cathode	Reversible potential	820 mV
	Activation potential	60 mV
	Effect of smoothing additives	2 mV
Anode	Reversible potential	1217 mV
	Oxygen overpotential	840 mV
	Scale effects	150 mV
	Additive effects	45 mV
	Silver alloy effect (0.5%)	- 80 mV
	Manganese effect	-190 mV
Conductivity - IR drop	Cathode sheet	2 mV
	Anode sheet	10 mV
	Contacts	24 mV
	Electrolyte potential drop	450 mV
	Gas bubble effect (10% of electrolyte)	45 mV
Total cell voltage		3395 mV

In recent years, it has been proposed to replace lead-based anodes with alternative anodes which are more energy efficient, offering low overvoltage for oxygen evolution reaction [8]. In some copper electrowinning plants, lead anodes have been replaced with coated titanium anodes. These anodes are called mixed metal oxide (MMO) anodes [10]. Coating of MMO anodes, which are usually $IrO_2.Ta_2O_5$, have some significant advantages. This coating has a lower overpotential for oxygen evolution than do the lead-based anodes. Subsequently, MMO anodes improve the energy efficiency by 15 % [11]. Moreover, MMO anodes eliminate the cobalt sulfate addition to the zinc electrolyte which was proposed to decrease the operation potential [9]. Using of MMO anodes improves the quality of zinc product by removing lead particles in zinc products. Also, this type of anodes offers a very good dimensional stability in the cell [12].

When using MMO anodes in zinc electrowinning process, presence of manganese ions in the electrolyte decreases energy efficiency significantly. Manganese ions are deposited on the surface of MMO anodes in the form of manganese dioxide. Manganese dioxide increases oxygen overpotential on the anode since MnO_2 is less electroactive than IrO_2 for oxygen evolution. MnO_2 deposited on the anode also decreases the lifespan of MMO anodes. The manganese concentration in typical electrolyte in copper electrowinning process is between (10 - 200) mg L^{-1} while this concentration in zinc electrolyte is between (2 – 5) g L^{-1} [13, 14]. Therefore, the zinc electrolyte conditions must be optimized for removing of manganese since the electrolyte contains high concentrations of manganese ions.

Hypothesis

Effect of manganese on zinc electrowinning process and methods for manganese removal has been reported in the literature and it is proposed that by removing manganese from zinc electrolyte before entering to the electrowinning cell, it could be possible to use MMO anodes in the zinc electrowinning cell and increase the energy efficiency.

This research proposes an auxiliary electrochemical system to remove manganese from the electrolyte before entering to the main electrowinning cell. In this system, manganese is oxidized to manganese dioxide and is removed from the electrolyte by deposition on the anode and precipitation in the operating cell. This system can be implemented at two locations in zinc electrowinning process i.e., after the purification stage to use the purified electrolyte or near to electrolysis stage to use the electrolyte of zinc electrolysis cell. The purified electrolyte is at 80 °C and pH 4 while the electrowinning solution is at 40 °C and pH 1.

The use of lead-based anode is one of the natural choices for such an auxiliary system due to the known performance and low cost of these electrodes. The optimum operating conditions at the two locations must therefore be determined to assess the technical and economic viability of the electrochemical purification system and in turn establish the best location for implementation. To answer these questions, we chose a commercial Pb-0.7 wt.% Ag anode as the target anode to study the effect of operating conditions such as pH, temperature and current density on Mn removal efficiency.

In this work, the effects of temperature and current density on manganese removal efficiency are studied at temperatures of 40, 60 and 80 °C, current densities of 65, 125, 250 and 500 A m^{-2} and pH of 1 and 4. These conditions were chosen according to the conditions of two targeted locations for implementation of the alternative manganese removal cell and conditions of electrolyte used industrially in that locations in zinc electrowinning process.

Based on the literature, the oxygen evolution on the surface of lead-silver is increased when the temperature and current density are increased. So, we hypothesize that the deposition rate of manganese on the lead-silver anode could be enhanced at lower temperatures and lower current densities, the latter being due to the competition between oxygen evolution reaction and manganese oxidation on the anode.

Chapter 1: Literature review

1.1 Overview of the Zinc production process

Basically, there are three types of zinc ores in the Earth's crust, oxidized, carbonated and sulfur including zinc ores. However, most zinc ores are in form of sulfur because they did not have enough time to be oxidized geologically [15].

Zinc sulfide ore, which is known as "zinc blende" or "sphalerite", is the most important mineral in zinc production while the other zinc ores are only of local importance. Zinc sulfide (ZnS) is composed of zinc, sulfur and small amount of other impurities such as Fe, Co, Cd, Mn, Cu, etc. [16, 17]. Table 1.1 presents the typical composition of common zinc minerals.

Table 1.1. Chemical composition of zinc minerals [18].

Mineral	**Formula**	**Zinc content %**
Sphalerite	ZnS	67.1
Marmatite (iron in solid solution)	(Zn, Fe) S	< 67.0
Smithsonite	$ZnCO_3$	52.2
Hydrozincite	$3ZnO.2ZnCO_3.3H_2O$	59.5
Willemite	$2ZnO.SiO_2$	58.7
Hemimorphite	$4ZnO.2SiO_2.2H_2O$	54.3
Zincite	ZnO	80.4

1.1.1 Zinc purification process

In order to obtain pure zinc from zinc sulfide ores, a series of purification steps are used including roasting, leaching, purification, and electrowinning. This series of process is most common method to produce zinc from zinc sulfide, and more than 85 % of the worldwide

zinc products are produced by this process [18]. Figure 1.1 shows the schematic representation of the zinc production process flowsheet.

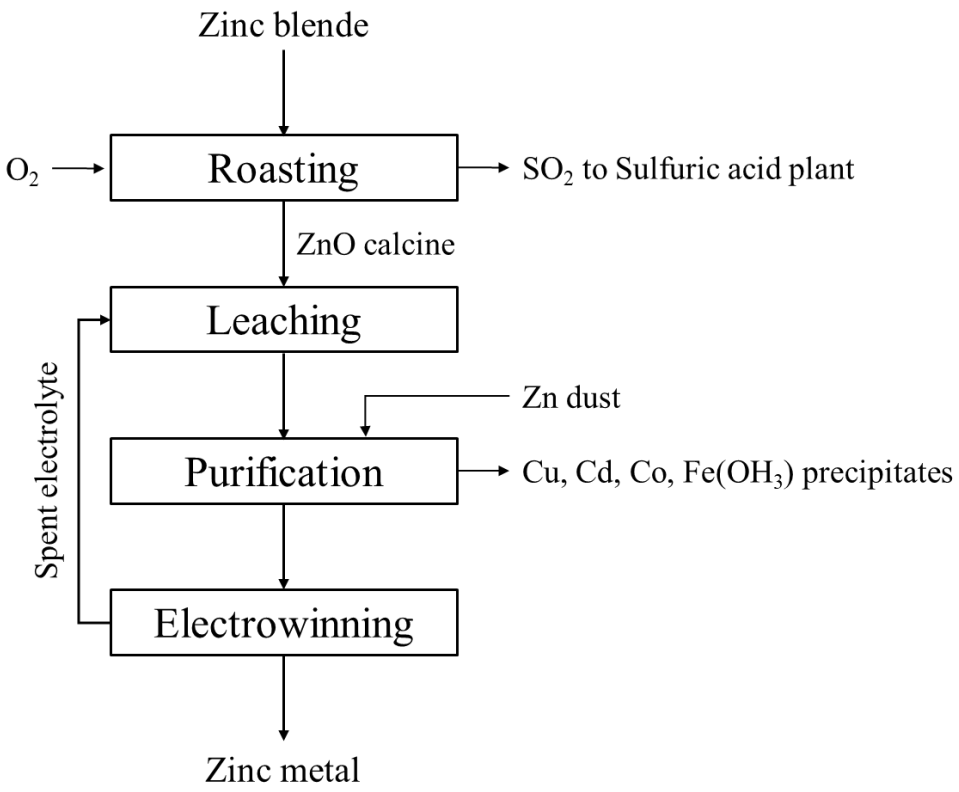

Figure 1.1. Flow chart of zinc purification process [3].

1.1.1.1 Roasting

In the first stage of the purification of zinc, sphalerite (ZnS), which is insoluble in dilute sulphuric acid, is first converted to soluble zinc calcine (ZnO) in roasters. The valuable by-product of this process is sulfuric acid [18, 19]. There are some main reactions involved in the oxidation of zinc sulfide concentrate, which are presented below (reactions 1.1 – 1.4). These combustion reactions are strongly exothermic, and the reaction equilibrium is controlled by the partial pressures of oxygen and sulfur dioxide. Oxygen is supplied by air [18].

$$ZnS + 2O_2 \rightarrow ZnSO_4 \quad (1.1)$$

$$3\,ZnS + 5.5\,O_2 \rightarrow ZnO.2ZnSO_4 + SO_2 \quad (1.2)$$

$$ZnS + 1.5O_2 \rightarrow ZnO + SO_2 \quad (1.3)$$

$$ZnS + O_2 \rightarrow Zn + SO_2 \quad (1.4)$$

The roasting process is carried out by circular hearth furnaces. In this process, crushed zinc sulfide is fed with air through a burner into a hot combustion space which is kept at about 950 °C. At these conditions, sulfur is eliminated almost completely. Sulfur in the roasted product my be present in the form of sulfide (0.1 – 0.4) % and sulfate (2 – 3) % [4, 18].

1.1.1.2 Leaching

In the leaching stage, the produced zinc oxide is dissolved in sulfuric acid (reaction 1.5). Sulfuric acid is supplied in the form of spent electrolyte after electrowinning and typically contains (150 – 200) g L^{-1} sulfuric acid and (48 – 56) g L^{-1} zinc above 90 °C. The spent electrolyte can be heated by heat exchange with steam and this can use the by-product steam from the roasting plant [4, 20].

$$ZnO + H_2SO_4 \rightarrow ZnSO_4 + H_2O \quad (1.5)$$

The leaching process is carried out in a series of agitated tanks (often with 5 tanks in series) to give a total residence time of the order of 5 to 6 hours. These tanks are generally acid brick lined for insulation and corrosion protection [18, 21]. Moreover, in leaching process, zinc is liberated as well as impurities such as iron, cobalt, copper, cadmium, and nickel. In order to obtain a pure zinc, leaching operation as a part of zinc purification process, must provide a suitable solution for electrowinning following appropriate purification procedures [22].

Iron in the calcine, which is in the form of zinc ferrite, can be dissolved in the leaching stage conditions ((150 – 200) g L^{-1} sulfuric acid at 90 °C) and 3 hours of residence time. The basic reaction of ferrite extraction is given in reaction 1.6 [18].

$$ZnO.Fe_2O_3 + 4\ H_2SO_4 \rightarrow ZnSO_4 + Fe_2(SO_4)_3 + 4H_2O \quad (1.6)$$

For many years, iron was precipitated as ferric hydroxide ($Fe(OH)_3$) by simple neutralisation method. This precipitation is gelatinous and difficult to separate by settling and filtration. Also, this method was only useful for precipitation of small quantities of iron, limited to

about 2 g L^{-1} [23]. Currently, it is more usual to precipitate iron as three iron compounds including jarosite (usually $(NH_4)_2\ Fe_6(S0_4)_4(OH)_{12}$) for ferric iron concentration more than 12 g L^{-1}, goethite (FeOOH) for ferric iron concentration above 2 g L^{-1} less than 12 g L^{-1} and haematite (Fe_2O_3) for ferric iron concentration less than 2 g L^{-1} [24]. The reactions of iron precipitation as jarosite, goethite and haematite are presented in reaction 1.7, 1.8 and 1.9, respectively [25].

$$3Fe_2(SO_4)_3 + (NH_4)_2SO_4 + 12H_2O \rightarrow (NH_4)_2Fe_6(OH)_{12}(SO_4)_4 + 6H_2SO_4 \quad 1.7$$

$$2\ FeSO_4 + ½\ O_2 + 3\ H_2O \rightarrow 2\ FeOOH + 2\ H_2SO_4 \quad 1.8$$

$$2\ FeSO_4 + 2\ H_2O + ½\ O_2 \rightarrow Fe_2O_3 + 2\ H_2SO_4 \quad 1.9$$

1.1.1.3 Purification

In the zinc electrowinning process, impurities coming from calcine must be removed in order to achieve the well purified electrolyte to subsequently being fed to electrowinning stage. So that it is necessary to carry out the purification operation. The purification process is carried out to remove elements that will co-deposit with zinc during electrolysis and hence contaminate the final product. Also, the purification stage must remove the elements which reduce the current efficiency of zinc electrodeposition by lowering the hydrogen overpotential [26].

To remove the elements higher on the electrochemical series than zinc, the elements are displaced from solution with metallic zinc which does not add any new components to the solution. This process which is called “cementation”, involves the treatment of impure solutions with zinc powder in an agitated tank. Generally, cementation process in the zinc purification process is carried out to remove some impurities including copper, cadmium, cobalt and nickel which are discussed later in more details. The other impurities can be removed if efficient separation of the target metals is achieved [27, 28]. Table 1.2 presents the concentration of typical impurities before purification (after leaching and iron removal) stage and after purification stage [3].

Table 1.2. Concentration of impurities in zinc purification process, before and after purification step.

Elements	Before purification (mg L^{-1})	After purification (mg L^{-1})
Zinc	100000 – 180000	110000 – 180000
Manganese	2500 – 20000	2500 – 20000
Cadmium	10 – 500	0.1 – 0.5
Copper	10 – 600	0.02 – 0.5
Iron	1 – 10	1 – 10
Cobalt	2 – 20	0.1 – 1.0
Nickle	1 – 10	0.02 – 0.1
Arsenic	0.1 – 0.5	0.1 – 0.2
Antimony	0.1 – 0.5	0.01 – 0.1
Germanium	10 - 100	0.001 – 0.01

Previous studies about purification stage and removing the impurities in zinc electrowinning process result that the typical optimum operating conditions for purification stage include 150 g L^{-1} Zn^{2+} at 80 °C, at pH 4, if the initial concentration range of impurities lays in the ranges presented in table 1.2. Also, the concentration of zinc is adjusted by adding the zinc dust in the electrolyte [3, 26].

Cadmium can co-deposit with zinc and contaminate the zinc products. To mitigate the negative effect of high concentration of cadmium in the electrolyte, zinc dust is added. The typical concentration of cadmium in the zinc electrolyte is around 0.7 mg L^{-1} while this concentration in the purified solution becomes less than 0.3 mg L^{-1}. The reaction of cadmium cementation is given in reaction 1.10 [29].

$$CdO + ZnSO_4 \rightarrow ZnO + CdSO_4 \qquad 1.10$$

Copper can deposit during zinc electrodeposition on the cathode and reduce the hydrogen overvoltage and subsequently decrease the current efficiency. Presence of 1 mg L^{-1} copper in the electrolyte can decrease the current efficiency by 5 %. Copper is removed by

cementation process and adding the zinc dust to obtain low concentration of copper, which is generally around 0.03 mg L^{-1} in the electrolyte. The reaction 1.11 presents the cementation reaction of copper with zinc [30].

$$CuSO_4 + Zn \rightarrow ZnSO_4 + Cu \qquad 1.11$$

Nickel reduces the current efficiency of zinc electrodeposition by making holes in the zinc electrowinning products and re-solution of the deposited zinc on the cathode. Nickel reduces the current efficiency of zinc electrowinning by 10 % when it is present in the electrolyte at a concentration of 10 mg L^{-1}. The typical concentration of nickel in the electrolyte is 0.1 mg L^{-1} and in order to keep the nickel concentration below this level, zinc dust is added. Nickel is removed with cobalt and it is cobalt that determines the operating conditions for their cementation. Nickel can be removed from electrolytic solution by cementation on zinc according to the reaction 1.12 [31].

$$Zn + Ni^{2+} \rightarrow Zn^{2+} + Ni \qquad 1.12$$

Cobalt is one of the most harmful impurities during zinc electrowinning. Presence of cobalt reduces the current efficiency, quality and purity of zinc deposition. Cobalt can co-deposit with zinc at the cathode due to its standard electrode potential (Table 1.3). The co-deposition of cobalt with zinc at the cathode acts as catalyst for hydrogen evolution reaction. The fast hydrogen evolution decreases the current efficiency of electrowinning stage and increases the energy consumption [22, 32]. Moreover, the co-deposition of cobalt with zinc makes holes on the zinc deposition and reduces the purity and quality of zinc deposition. Also, this co-deposited cobalt can enhance the dissolution of zinc by forming micro-galvanic cells with zinc [33, 34].

The cementation reaction of cobalt is very slow due the kinetic barriers, so that the cementation of cobalt requires the activators. It has been found that cobalt cementation can be improved considerably by using activators which increase the rate of cobalt cementation by increasing the hydrogen overpotential at the cathode [35]. There are two main cobalt cementation methods which are used in the industry: activation with arsenic and copper or

with antimony and copper. Reaction 1.13 and 1.14 show the cobalt cementation reaction in the zinc electrolyte by Cu-Sb activators and Cu-As activators, respectively [35, 36].

$$2Co^{2+} + 2HSbO_2 + 5Zn + 6H^+ + 20e^- \rightarrow 2CoSb + 4H_2O + 5Zn^{2+} \quad 1.13$$

$$2Co^{2+} + 2HAsO_2 + 6H^+ + 5Zn \rightarrow 2CoAs + 4H_2O + 5Zn^{2+} \quad 1.14$$

The optimized experimental condition for cobalt cementation at the presence of Cu-sb was reported by Raghavan *et al.* (1999) [37], i.e., 150 g L^{-1} Zn^{2+}, Sb^{3+} 1 mg L^{-1}, 25 mg L^{-1} Cu^{2+}, pH between 4.5 to 4.6 and temperature 80 °C to 85 °C and a reaction time of 3 hours to 3.5 hours. However, Tozawa *et al.* (1992) [36], have reported that the best conditions for cobalt cementation in the presence of Cu-As are obtained with 150 g L^{-1} Zn^{2+}, 10 mg L^{-1} Co^{2+}, 20 mg L^{-1} As^{3+}, at pH 3.3 at 90 °C and a reaction time of 200 minutes.

1.1.1.4 Zinc electrowinning

In the zinc electrowinning stage, zinc ions are discharged from a zinc sulfate solution at the cathode of an open electrolytic cell. There is always a competing reaction at the cathode between discharge of zinc for zinc deposition and discharge of hydrogen to release hydrogen. The reactions of zinc deposition and hydrogen evolution on the cathode as well as oxygen evolution reaction on the anode are given in the reactions 1.15, 1.16 and 1.17, respectively. Moreover, the reaction 1.17 shows that the decomposition of water on the anode regenerates sulfuric acid in the electrolyte [38-40].

$$Zn^{2+} + 2e^- \rightarrow Zn^0 \quad , E°_{cathode}\,(SHE) = -0.763\ V \quad 1.15$$

$$2H_3O^+ + 2e^- \rightarrow 2H_2O + H_2 \quad , E°\,(SHE) = 0.005\ V \quad 1.16$$

$$6H_2O \rightarrow O_2 + 4H_3O^+ + 4e^- \quad , E°_{anode}\,(SHE) = -1.23\ V \quad 1.17$$

Finally, the overall reaction in the cell can be written as:

$$Zn^{2+} + 2H_2O \rightarrow 2Zn + O_2 + 4H^+ \, , E°_{cell}\,(SHE) = -1.993\ V \quad 1.18$$

Overall theorical cell potential becomes as below [40]:

$E°_{cell} = E°_{anode} + E°_{cathode} = (-1.23\ V) + (-0.76\ V) = -1.993\ V$

In the zinc electrowinning cell, aluminium acts as cathode and lead-silver alloy as anode [40]. Figure 1.2 shows the schematic representation of a zinc electrowinning cell.

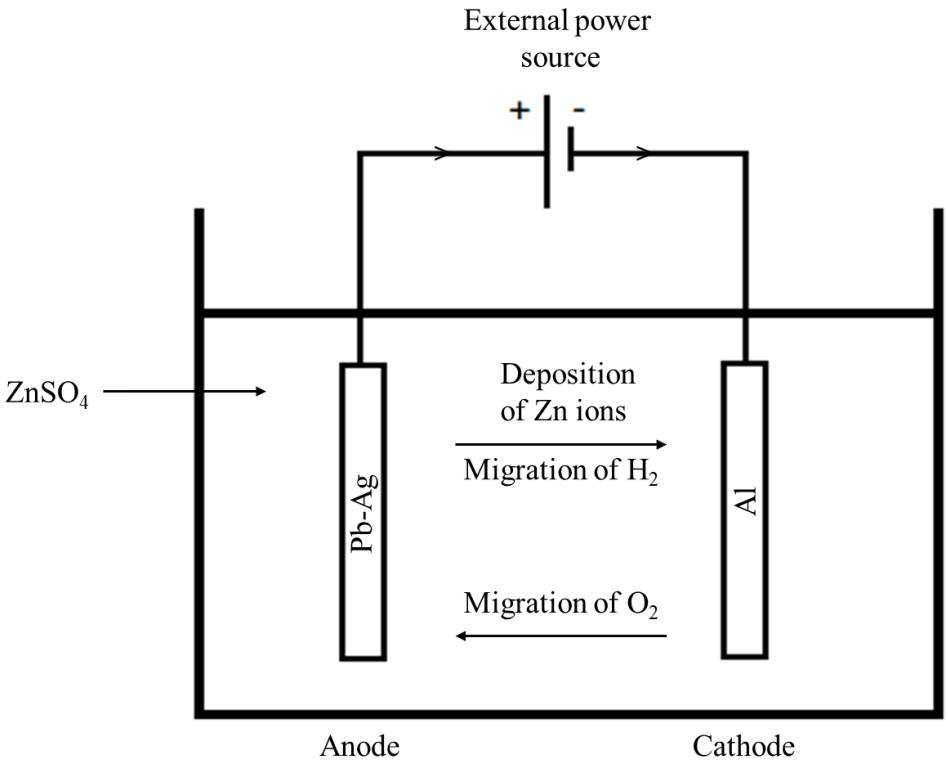

Figure 1.2. Electrolytic cell for performing zinc electrowinning process [40].

Table 1. 3. Standard electrode potentials (relative to the H^+ electrode at 25 °C) [41].

Electrode Reaction	Potentials (E°) volts
Mg / Mg^{2+}	-2,363
Sc / Sc^{3+}	-2,077
Be / Be^{2+}	-1,847
Al / Al^{3+}	-1,660
Mn / Mn^{2+}	-1,179
Cr / Cr^{2+}	-0,913
Zn / Zn^{2+}	-0,760
Fe / Fe^{2+}	-0,440
Cd / Cd^{2+}	-0,400
Co / Co^{2+}	-0,277
Ni / Ni^{2+}	-0,250
Sn / Sn^{2+}	-0,136
Pb / Pb^{2+}	-0,126
H_2 / H^+	0,000
Sb / Sb^{3+}	+0,2
Bi / Bi^{3+}	+0,23
Cu / Cu^{2+}	+0,337
Hg / Hg^+	+0,788
Ag / Ag^+	+0,799
Pd / Pd^{2+}	+0,987
Pt / Pt^{2+}	+1,188
Au / Au^+	+1,692

Table of standard electrode potentials (Table 1.3) shows that zinc has a more negative standard electrode potential than hydrogen, so that hydrogen ions should be discharged at the cathode and electrodeposition of zinc should not be possible. However, the given standard potentials in Table 1.4 are under reversible conditions (where forward and reverse reactions are in equilibrium) at no current flow. By applying the electrical current density in an electrolyte, the reaction at the cathode surface is restricted and this restriction can be overcome when the applied electrode voltage is increased. The difference between the increased potential required and the reversible electrode potential is defined as overpotential or overvoltage [42].

The hydrogen overpotential in zinc electrowinning process at typical operating conditions (which are defined later) results to change the potential of hydrogen evolution from +0.005 V to -1.109 V (i.e., the electrode potential become -1.104 V) and limiting the reaction 1.16 in favour of reaction 1.15 on the cathode, i.e., the overall electrode potential for deposition of hydrogen is more negative than potential for the deposition of zinc, hence zinc is preferentially deposited [43]. Presence of impurities in the zinc electrolyte, can make different hydrogen overpotentials. The impurities can co-deposit with zinc and reduce the hydrogen overpotential, i.e., the co-deposition of impurities with zinc on the cathode results to change the system in favour of hydrogen evolution and reduce the current efficiency of zinc deposition [44]. Moreover, there are some factors which they influence the electrode potential, such as current density, zinc concentration and temperature.

The studies around the effect of current density on zinc deposition show that at low current densities, hydrogen is preferentially deposited, but at higher current densities the hydrogen overpotentials is increased and zinc is preferentially deposited. However, there is a limitation to increase the current density due to the diffusion of zinc [45]. The limiting current density is determined by equation 1.1 [46].

$$j_{LIM} = \frac{nFD_Z C_B}{\delta} \qquad \text{Eq. 1}$$

Where:

n is the number of electrons involved per mole (for Z^{2+} is 2)

F is Faraday constant = 96500 coulombs per mole (C mol^{-1})

D_Z is the diffusion coefficient for zinc (0.5×10^{-5} cm^2 s^{-1})

C_B is the bulk solution concentration of zinc

δ is the thickness of the boundary layer

For any zinc electrolyte, there is an optimum current density that is the balance between minimum of hydrogen overpotential and limiting diffusion current for zinc. Also, the concentration of zinc in the solution can affect the current density. In high zinc concentration electrolyte, the current density of limiting zinc current is increased. Figure 1.3 shows the electrode potential-current relationship for zinc deposition and hydrogen evolution, limiting zinc current and effect of zinc concentration. Overall, in operating conditions the optimum current density is between 400 A m^{-2} to 500 A m^{-2} [46].

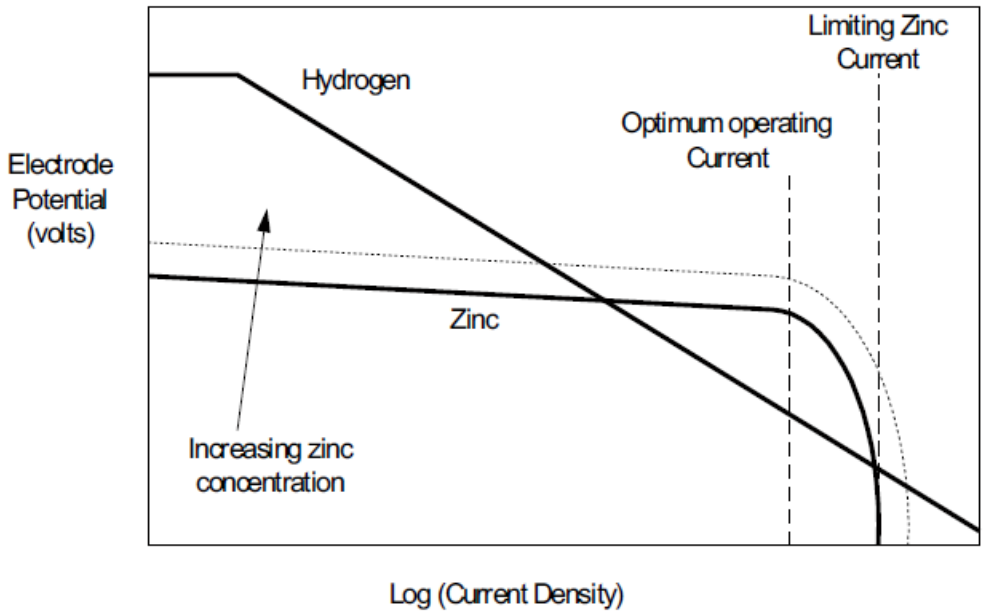

Figure 1.3. Electrode potential-current relationships for zinc and hydrogen. Showing limiting current and concentration effects [46].

Moreover, for a given current density, an increase in temperature results an increase in the electrode potential and limiting the effect of overvoltage. By decreasing the overvoltage, the competing reaction between hydrogen deposition and zinc deposition turns to favour of

hydrogen deposition and decrease the current efficiency of zinc deposition. However, the electrical conductivity of the electrolyte increases with temperature. An increase in electrical conductivity results in the decrease of the potential drop in the electrolyte and reducing the energy consumption. Hence, according to these two opposing effects, there is an optimum operating temperature to give a minimum energy consumption per unit of zinc deposited. Generally, the optimum operating temperature corresponding to the purity of solution is between 36 °C to 46 °C [47, 48].

Finally, Scott *et al.* (1988) [49], studied the optimum operating conditions of zinc electrowinning cell and they reported that the optimal conditions include 70 g L^{-1} Zn^{2+}, 180 g L^{-1} H_2SO_4, at 400 A m^{-2}, at 45 °C for 72 h of electrolysis and in this conditions the total cell voltage was 2.6 V. However, in the recent years, the typical operating conditions of electrowinning cell became as 55 g L^{-1} Zn^{2+}, 170 g L^{-1} H_2SO_4, at 500 A m^{-2} and at 40 °C for 48 h of electrolysis [50, 51]. James *et al.* (2000) [52], studied the zinc electrowinning at the recent conditions and they reported that the cell voltage was 3.5 V and the final current efficiency of zinc deposition was 90 %.

1.2 Manganese in zinc electrowinning process and its effects

Manganese is the third most abundant transition metal in Earth's crust and element 25 of the periodic system. The atomic weight of manganese is 54.94, the melting point is 1244 °C and the boiling point is 2060 °C [53]. Moreover, manganese is a metal impurity found in zinc ores and its concentration could reach 15 g L^{-1}. The presence of manganese in zinc electrowinning process is generally undesired, however it may exhibit positive effects in the electrolysis process when its concentration is within a certain range. Manganese ions in the electrolyte are oxidized at the anode to form permanganate (MnO_4^-) and then manganese dioxide (MnO_2) [54, 55].

As it will be discussed later in this chapter, the main objective of the industry is to replace the lead anodes by the MMO anodes. The MMO anodes can potentially result in lower cell voltage, thus offering better energy efficiency of the process. However, one of the main obstacles for using MMO anodes in zinc electrowinning process is the presence of Mn in the electrolyte. MnO_2 could deposit on the MMO anode. We anticipate that MnO_2 can damage

the MMO anodes or reduce their catalytic activity. It is therefore important to control the Mn concentration in the electrolyte, when the MMO anodes are used. This is the reason why, in the following two sections, we focus on the effect of Mn on the overall electrowinning process and the means by which it could be removed.

1.2.1 Positives effects

During the zinc electrowinning process, lead anodes are corroded and contaminate the zinc product on the cathode. Presence of (1 – 3) g L^{-1} manganese reduces the corrosion rate of lead anode and contamination of zinc products with lead. This is proposed by depolarizing effect of MnO_2 layer formed on the anode. [56, 57]. In the absence of manganese, corrosion rate is highly independent of current density, but in the presence of manganese corrosion rate is decreased by decreasing the current density [58].

The zinc electrolyte have usually some amounts of chlorine ions [59]. Chlorine ions attack lead anode and increase their corrosion rate. Manganese dioxide deposition on the anode, prohibits diffusion of chlorine ions to the anode, thus offering a certain level of protection against anode corrosion [58].

Due the overpotential in the zinc electrowinning process, some impurities such as copper, cobalt, nickel, and antimony can have a polarization effect in the electrolyte. These impurities are more electropositive than zinc, and they can cause re-dissolution of zinc from cathode [60]. In the presence of manganese in the electrolyte, the deleterious effect of above impurities is decreased. This is proposed that the manganese hydrates block the active hydrogen sites of the impurities on the zinc cathodic surface. Thus, the process of zinc re-dissolution is inhibited and this effect is occurred at high temperature. [61, 62].

1.2.2 Negative effects

Presence of manganese of more than 3 g L^{-1} in the electrolyte decreases the current efficiency of zinc deposition and increases the size of zinc platelets. Manganese in the form of MnO_2 (which is produced on the anode) can also deposit on the cathode. The manganese dioxide

deposited on the cathode, may anodically dissolve zinc from the cathode by forming galvanic pair with zinc and increase the energy consumption [57, 63].

A good electrical conductivity between anode and cathode, is one of the important factors for increasing the product yield of zinc electrowinning process. Presence of manganese in the electrolyte and deposition of that on the anode, as manganese dioxide, can make an oxide layer on the anode, reduce the electrical conductivity in the solution and decrease current efficiency of zinc deposition [64].

Moreover, concentration of manganese of more than 4 g L^{-1} makes a thick and sticky layer of manganese dioxide on the anode, which must be cleaned periodically. This reaction increases the frequency of anode cleaning. Also, a layer of manganese dioxide cannot be removed without losing a part of the anode surface [65].

1.3 Manganese control methods in zinc electrowinning

Manganese in the electrolyte can be controlled in various methods such as oxidative precipitation, hydroxide precipitation, evaporation, solvent extraction, and electrowinning [66]. A summary of oxidative precipitation and electrowinning methods are presented below.

1.3.1 Oxidative precipitation

Oxidative precipitation is a method to remove manganese as insoluble manganese oxides from zinc, copper and nickel processing circuits. The main form of manganese oxide in the oxidative precipitation method is manganese dioxide (MnO_2). Manganese dioxide is a strong oxidising agent which needs a stronger oxidant to oxidise Mn^{+2}. Manganese (II) is oxidised to higher valances, initially to manganese (III) and then to manganese dioxide. In this method, various oxidants are used such as ozone, catalysed SO_2/O_2 mixture, and persulfate [66].

1.3.1.1 Oxidation by ozone

Ozone (O_3) is an allotropic form of oxygen. The electron density causes it to be a strong oxidation agent which can oxidise manganese [67]. By adding ozone to the zinc electrolyte

with a concentration of manganese higher than 15 g L^{-1}, manganese can be oxidised and precipitate (Reaction 1.19) [68].

$$O_3 + Mn^{2+} + H_2O \rightarrow MnO_2 + O_2 + 2H^+ \quad 1.19$$

Bolton *et al.* (1983) [69], patented a process for removing manganese and chloride ions from aqueous acidic zinc sulfate solutions containing zinc, manganese and chloride ions without removing a substantial amount of zinc ions from the solution. They reported that in this process, acidified aqueous $ZnSO_4$ solutions are treated with ozone to oxidize manganese ions to manganese dioxide and the precipitated manganese dioxide is removed from the solution. Also, the chloride was removed as chlorine gas from the solution. This process was carried out to treat the spent electrolyte from H_2SO_4 leaching of ZnS ores. In this process, O_2 containing 57.5 mg L^{-1} O_3 was passed through a solution containing 150 g L^{-1} H_2SO_4, 50 g L^{-1} Zn^{2+}, 3.74 g L^{-1} Mn^{2+} and 107 mg L^{-1} Cl^- at 23 °C. The ozone was passed in countercurrent flow to the solution flow. They achieved that the manganese and chloride ion concentrations after this process were 0.03 g L^{-1} and 3 mg L^{-1}, respectively.

In a study by Ichlas *et al.* (2020) [70], a method using oxidative precipitation by ozone for processing mixed nickel-cobalt hydroxide precipitate to separate nickel from cobalt and manganese was proposed. They demonstrated that complete precipitation of cobalt and manganese can be achieved using ozone as oxidant with nickel co-precipitation of about 8.8 % at 25 ˚C, equilibrium pH of 5, oxidant gas flow rate of 1 L min^{-1} and precipitation duration of 2 h.

Generally, the application of oxidation by ozone is in the water treatment plants and use of this method for manganese removal in the zinc electrowinning process is limited to laboratory scales [71]. However, the ozone oxidant is an effective but rather expensive oxidant for manganese and thus is less feasible than cheaper oxidants such as SO_2/O_2 mixture [72].

1.3.1.2 Oxidation by SO_2/O_2 mixture

Sulfur dioxide/oxygen (SO_2/O_2) mixture is one of the strong oxidants at a correct ratio for manganese ions. This oxidant is cheap and easy to make or extract from smelter off-gas. In this oxidation process, as presented by Zhang *et al.* (2002) [72], manganese is precipitated in

the two forms of MnO_2 and Mn_2O_3 in the pH range of 3 to 6 and temperature range of 25 °C to 80 °C. The rate of manganese oxidation with SO_2/O_2 mixture is first order with respect to SO_2 partial pressure up to 5.7 % SO_2 at 80 °C and half order with respect to $[H^+]$. The rate of oxidation of manganese is slow at pH less than 3 and increases rapidly at pH above 4. This mixture also oxidises zinc (at pH 3 to 4), cobalt (at pH 5) and nickel (at pH 7) [73].

The precipitation of manganese as two forms of MnO_2 and Mn_2O_3 with SO_2/O_2 mixture oxidant is carried out as following reactions [74].

$$2Mn^{2+} + SO_2 + O_2 + 3H_2O \rightarrow 2MnO(OH) + SO_4^{2-} + 6H^+ \quad 1.20$$

$$Mn^{2+} + SO_2 + O_2 + 2H_2O \rightarrow MnO_2 + SO_4^{2-} + 4H^+ \quad 1.21$$

Ferron (2000) [75], reported that manganese could be effectively separated as precipitated manganese dioxide from zinc solutions with optimum mixture of SO_2 (0.5 – 10) % and O_2 at 40 to 80 °C and pH 3 - 5, preferably pH 3 - 4 to minimise loss of zinc by coprecipitation.

Another study using this technique for manganese removal is the one performed by Pérez-Garibay *et al.* (2018) [76], who demonstrated a reaction mechanism describing oxidative precipitation of Mn^{2+} by an SO_2/O_2 mixture with MnO_2 and SO_4^{2-} as reaction products. They performed the experimental conditions including 1.5 L of a purified leaching solution of a low grade pyrolusite ore (MnO_2) with an Mn content of 1500 ppm, in a 2 L glass reactor equipped with internal baffles to provide a vigorous agitation and each experiment was carried out at 25 °C and at pH 6. A gas flow of 200 mL min^{-1} was added with different gas compositions between 0 and 44.7 % SO_2 v/v to estimate the optimal composition gas mixture. They found that this system is efficient at low concentration of 7.3% SO_2 of the gas mixture.

The SO_2/O_2 oxidant is the cheap oxidant and where the process involves roasting zinc sulfide concentrates, this oxidant is the most applicable one. However, to enable this mixture to oxidise the manganese, it needs more analytical and automatic control for operation such as optimum solution pH and optimum SO_2/O_2 ratios. The rate of manganese oxidation with SO_2/O_2 as an oxidant is very slow in pH value of below 3 while the operating condition of zinc electrowinning process has more performance in lower pH. Also, there are significant

problems of scale-up of reactors for SO_2/O_2 (or air) precipitation due to the differing solubilities of the gases [77-79].

1.3.1.3 Oxidation by persulfate

Persulfates are also oxidation agents to remove manganese ions from zinc electrolyte. Persulfates such as peroxy-disulfuric acid ($H_2S_2O_8$) and peroxy-monosulfuric acid (Caro's acid), precipitate manganese ions in the form of manganese dioxide. The reactions 1.22 and 1.23 present oxidation reaction of manganese by persulfates oxidants [80, 81].

Oxidation by peroxy-disulfuric acid:

$$Mn^{2+} + H_2S_2O_8 + 2\,H_2O \rightarrow MnO_2 + 2\,H^+ + 2\,H_2SO_4 \qquad 1.22$$

And oxidation by Caro's acid:

$$Mn^{2+} + H_2SO_5 + H_2O \rightarrow MnO_2 + 2\,H^+ + H_2SO_4 \qquad 1.23$$

Burkin and Chouzadjian (1983) [81], used the Caro's acid for recovery of manganese from a zinc electrolyte containing 150 g L^{-1} Zn^{2+} and 6 - 7 g L^{-1} Mn^{2+}. They developed the process for oxidation of manganese (II) to manganese (IV) at pH 2, at (70 – 90) °C with (110 – 160) % of stoichiometric amount of Caro's acid relative to stoichiometric amount of manganese. The process of separation of precipitated manganese dioxide from the solution was also developed at Caro's acid/H_2O_2 ratio of 30:1. They reported that 70 % to 80 % manganese was precipitated.

A hydrometallurgical process was developed by Wang and Zhou (2002) [82], for the recovery of cobalt from a zinc plant residue. In this process, ammonium peroxy-disulfate ($(NH_4)_2S_2O_8$) was used for oxidative precipitation of iron and then manganese as MnO_2. Iron and manganese were precipitated completely at pH range of 3.5 to 4.5 at 95 °C for 1 h and 40 minutes with dropwise addition of 10 % ammonium peroxy-disulfate solution. To avoid the effect of ammonium peroxy-disulfate on dropdown of pH which can affect the precipitation of manganese and iron, a dilute sodium carbonate solution was added. The

concentration of manganese before the experiments was 130 mg L^{-1} which reached 0.3 mg L^{-1} in the final solution.

The main concern for the use of oxidative precipitation method for manganese oxidation is the cost of oxidants. Caro's acid and peroxy-disulfuric acid are expensive oxidants and use of these oxidants to oxidise manganese in zinc electrowinning process does not support the logic of process efficiency [83].

1.3.2 Electrowinning technique

In zinc electrowinning process, manganese is oxidized to MnO_2 and manganese dioxide is deposited on the anode. This process can be used as a method to remove manganese from electrolyte. In manganese oxidation process, firstly, manganese ions in the electrolyte are oxidized at the anode to form permanganate (MnO_4^-) and then by reaction of manganese (II) with permanganate results the formation of manganese (IV). Manganese (IV) is not stable in the solution and will react with water to form manganese dioxide. The reactions 1.24 to 1.26 present the formation of manganese ions to manganese dioxide [65, 84].

$$Mn^{2+} + 4\,H_2O \rightarrow MnO_4^- + 8\,H^+ + 5e^- \qquad 1.24$$

$$2\,MnO_4^- + 3\,Mn^{2+} + 16\,H^+ \rightarrow 5\,Mn^{4+} + 8\,H_2O \qquad 1.25$$

$$Mn^{4+} + 2\,H_2O \rightarrow MnO_2 + 4\,H^+ \qquad 1.26$$

The summary of above reactions for oxidation of manganese (II) to manganese dioxide become as reaction 1.27:

$$Mn^{2+} + 2H_2O \rightarrow MnO_2 + 4H^+ + 2e^- \;,\; E°_{anode}\,(SHE) = 1.228\ V \qquad 1.27$$

The anode is made of lead alloys or graphite and oxygen is evolved during deposition of manganese on the anode. On the other side, zinc is reduced and deposited on the aluminum cathode and hydrogen is evolved. The reactions 1.28 and 1.29 show the main reactions of deposition cathode and the overall cell reaction [85, 86].

Zinc deposition on the cathode:

$Zn^{2+} + 2e^{-} \rightarrow Zn$, $E°_{cathode}$ (SHE) = -0.763 V 1.28

Overall cell reaction is written as:

$ZnSO_4 + MnSO_4 + 2H_2O \rightarrow Zn + MnO_2 + 2H_2SO_4$, $E°_{Cell}$ (SHE) = 0.465 V 1.29

A study by Shaw *et al*. (2000) [87] demonstrated the removal of manganese using a process practiced in zinc electrowinning purification. The process involves reacting manganous ions in solution with permanganate ions. Reaction between these two produces insoluble manganese dioxide reaction product. This process has been carried out in a solution containing 1 g L^{-1} Mn^{2+}, 180 g L^{-1} H_2SO_4, 40 g L^{-1} Cu^{2+}, 2 g L^{-1} Fe^{3+} and 150 mg L^{-1} Co^{2+} at 45 °C. They reported that the final concentration of manganese in the electrolyte was 58 mg L^{-1}.

The oxidation of manganese by means of electrowinning method is one of the best ways to remove manganese from zinc electrolyte. This process can be applied to treatment of a bleed stream of zinc electrolyte containing a sufficiently high concentration of manganese or the same zinc electrowinning cell and electrolyte can be used to remove manganese by just changing the conditions such as current density and temperature. This method does not change acidity conditions significantly and manganese recovered can be of high-quality manganese dioxide under well-controlled conditions [86, 88].

This research is focused on exploring the possibility of removing manganese from the zinc electrolyte using lead-based anodes, with the aim of providing suitable conditions for using MMO anodes. In the last sections, techniques for manganese removal have been discussed. Electrowinning was chosen as a potential technique according to its advantages which are better suited for industrial applications i.e., not changing the range of conditions significantly from the zinc electrowinning cell.

Chapter 2: Materials and methods

In this work, it was attempted to remove manganese from zinc electrolyte means using electrolysis method and galvanostatic technique. Figure 2.1 shows the schematic representation of our electrowinning cell. This section presents the various components of electrolysis cell such as anode, cathodes, reference electrode as well as electrolytes and their compositions. Moreover, the techniques for manganese removal are described. Later, the characterization methods also are presented.

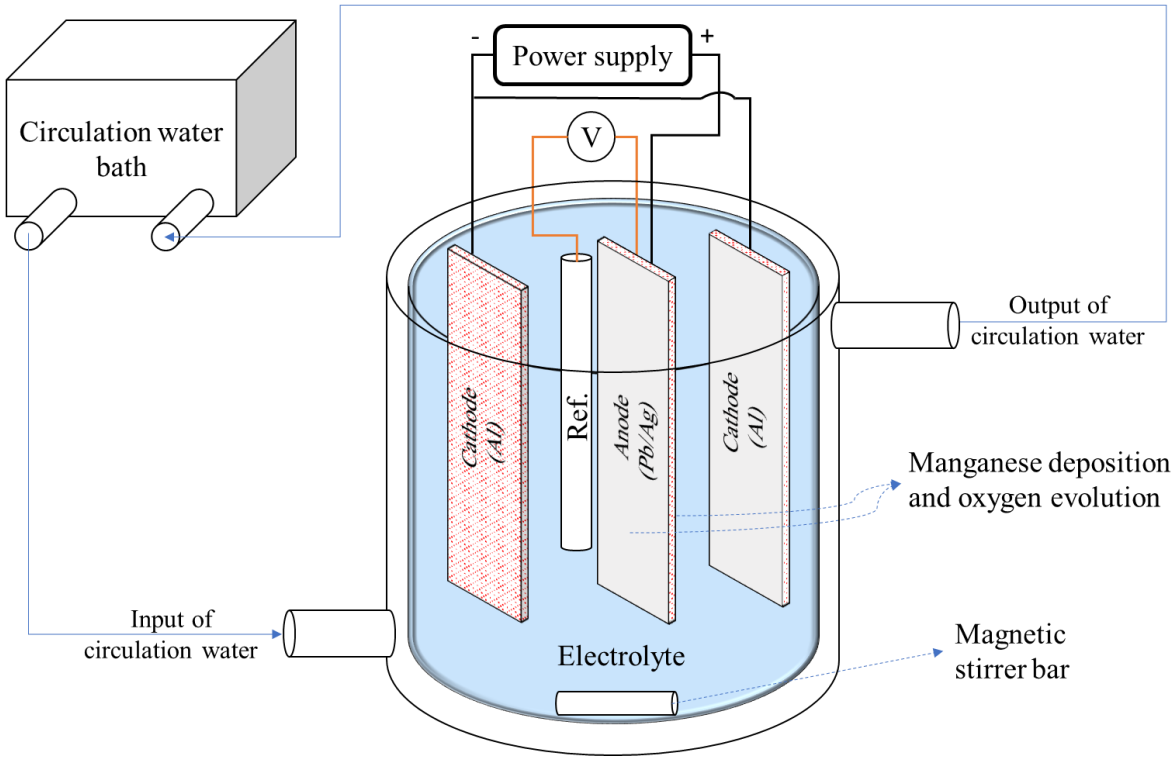

Figure 2.1. Schematic of manganese removal system cell

2.1 Cell components and experimental conditions

2.1.1 Anode

In any electrowinning process, the useful anode material must meet these requirement [89]:

1) They must have good electrical conductivity due to energy efficiency.
2) They must have good electrocatalytical properties to improve product yield.
3) They must be stable and have good resistance in long-term experiments, because corrosion contaminates the products thereby increasing energy consumption.

For a long time, lead and lead alloys as a natural choices have been used as anode in electrowinning process. Pure lead anodes have disadvantages to compare with lead alloy anodes. Pure lead cannot decrease oxygen overpotential sufficiently and may increas energy consuming. By using the pure lead in electrowinning process, it tends to creep and wrap. Also, pure lead has a low melting point due to use for casting. Moreover, pure lead is very ductile material and it can be machined easily. As a result, lead must be alloyed to improve mechanical properties [90].

In this work lead-0.7 wt.% silver is chosen as anode. By adding silver to pure lead and make the lead-silver alloy, following features are provided [91]:

1) Decreasing the oxygen overpotential and increasing energy efficiency.
2) Decreasing the anode potential and improving the electrical conductivity.
3) Increasing the corrosion resistance during the electrowinning process.
4) Increasing the anode's life and decreasing lead contamination in the cathode product.

2.1.2 Cathode

Aluminum is chosen as cathode because [92]:

1) Aluminum has a high overpotential and increases electrical conductivity in the electrolyte.
2) Aluminum does not form any alloy with the which is deposited on that.
3) Also, due the low density of aluminum, it is easy to handle.

2.1.3 Reference electrode

Silver chloride (Ag, AgCl/KCl_{sat}; 0.197 V versus SHE) is used as the reference electrode to measure the voltage of anode. As shown in figure 2.1, the reference electrode always was kept near to the anode surface during the experiments.

2.1.4 Electrolyte composition

To remove manganese from electrolyte in zinc process, two electrolyte conditions have been used. First is the purification solution which comes from purification stage and second is electrowinning solution which is used for electrowinning stage.

Purification solution is in the following conditions: zinc concentration 150 g L^{-1}, temperature 80 °C, and pH 4. The conditions for electrowinning solution are: zinc concentration 55 g L^{-1}, temperature 40 °C, and pH 1. Both solutions have been examined to find best conditions to remove manganese. Figures 2.2 and 2.3 show the schematic manganese control system in purification and electrowinning conditions, respectively.

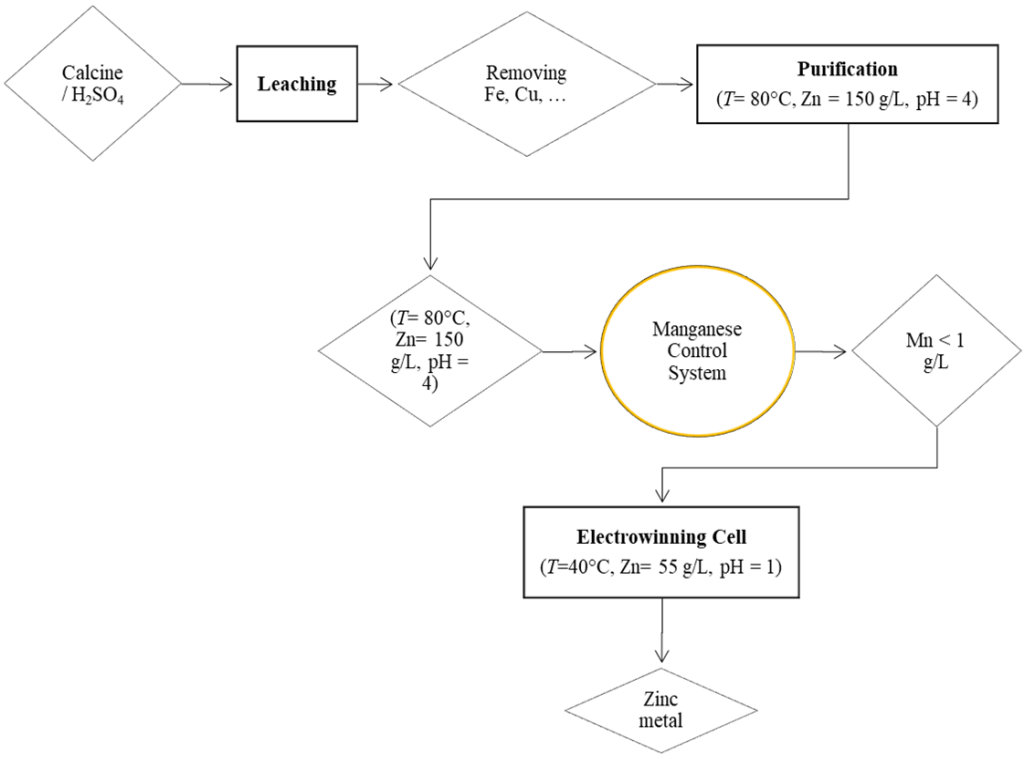

Figure 2.2. Schematic of manganese control system by using conditions of purification electrolyte.

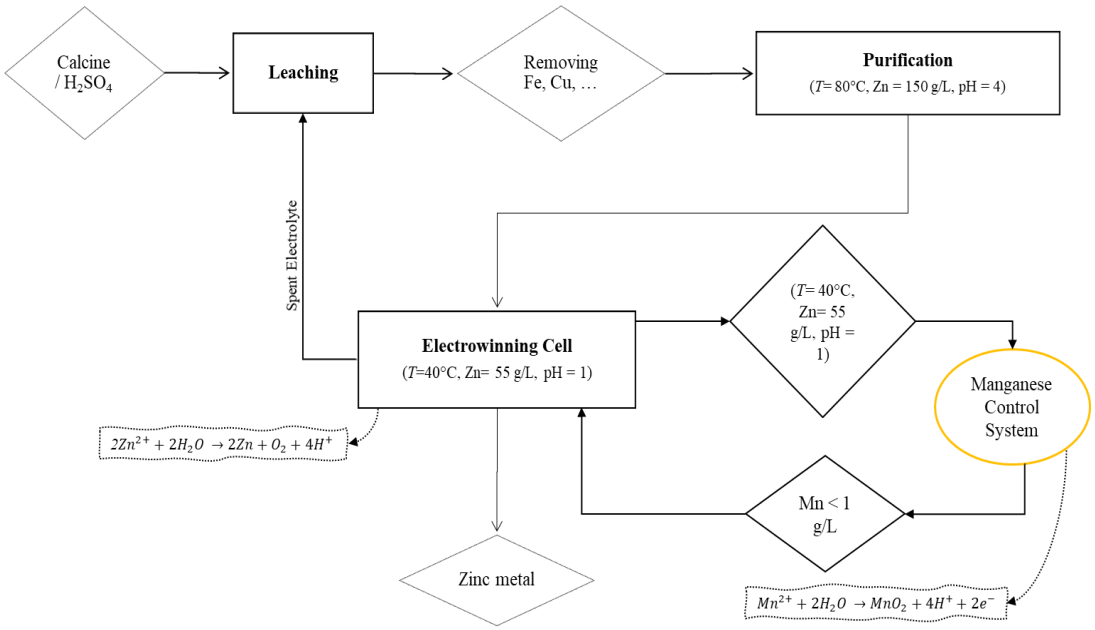

Figure 2.3. Schematic of manganese removal system by using conditions of electrowinning solution.

2.1.5 Current density, temperature and manganese concentration

To obtain the optimum conditions for manganese removal, different current densities and temperatures have been applied in both purification and electrowinning conditions. Current densities were 65, 125, 250 and 500 A m^{-2}. Temperatures were 40, 60, and 80 °C.

Also, the solutions have been made by different manganese concentrations such as 0.1, 0.5, 1, 2, and 4 g L^{-1} to investigate the effect of manganese concentration on manganese deposition rateon the anode, current efficiency, and anodic voltage.

2.1.6 Current efficiency

To calculate the current efficiency of manganese deposition, equation 2.1 is used.

$$CE\ (\%) = \frac{m_{\text{real}}}{m_{\text{th}}} \times 100 \qquad \text{Eq. 2.1}$$

In this equation, *CE* presents current efficiency, m_{real} is actual Mn deposited on the anode. The actual Mn deposit is calculated using the variation of the Mn in electrolyte, obtained by

Microwave Plasma Atomic Emission spectroscopy (MP-AES) analysis. m_{th} is the therocial Mn deposit which is obtained by equation 2.2.

$$m_{th} = \frac{MAit}{ZF} \quad \text{Eq. 2.2}$$

Where M represents atomic mass (g mol^{-1}), A surface of the anode (m^2), i applied current density (A m^{-2}), t time of deposition (s), Z electron number (i.e., for Mn^{2+} is 2) and F Faraday number (C mol^{-1}).

2.2 Electrochemical tests

2.2.1 Galvanostatic

Galvanostatic technique has been applied to investigate current efficiency and anodic overpotential. In this technique, power supply applies current in the circuit which includes anode, cathode, electrolyte, and wiring. By applying the current, manganese is deposited on the anode and zinc is deposited on the cathode. Figure 2.4 shows the typical manganese deposition on the anode surface, as a black propus powder. The tests were carried out for 2 hours and the samples were taken each 30 minutes from the electrolyte. To analyse the samples by Micro Plasma-Atomic Emission Spectroscopy (MP-AES) and find the concentration of manganese in the electrolyte, the sapmles were diluted with HNO_3 5 % and dilution factore was 100. Figure 2.5 shows the cell of galvanostatic tests.

Figure 2.2. Lead-silver anode, showing manganese deposition.

Figure 2.3. Cell of manganese removal system, using the galvanostatic technique.

2.2.2 Linear sweep voltammetry (LSV)

Linear sweep voltammetry technique was used to investigate the mechanism of oxidation reactions on the anode by generating peaks on the LSV curves. These tests were carried out using Al as auxiliary electrode, Pb-0.7%Ag as working electrode and a silver chloride as reference electrode. All electrodes were mounted in a Teflon holder set-up. Both electrodes were casted in polyester resin with an exposed surface area of 1 cm^2. A GAMRY® interface 1010E potentiostat was used to record log potential and current values. The LSV tests were performed over a range of potential (0.5 V to 2.0 V) using a potential sweep rate of 10 mV s^{-1} under atmospheric condition, with agitation rate of 200 rpm. All polarization tests were carried out at 40 °C in atmospheric conditions under agitation (200 rpm) using a potential sweep rate of 10 mV s^{-1}. Each sequence test started with an open circuit potential (OCP) condition for 10 seconds and then a LSV experiment.

2.3 Characterization

Analytical techniques have been used to characterise many aspects of the manganese samples. These include MP-AES for determining concentration of manganese and zinc in the electrolyte. For the powder deposited samples, XRD was used for the determination of manganese and other elemental compositions, elemental concentration was determined by XRF, and surface morphology mapping performed using SEM. The analytical techniques will be described in detail in the subsequent sub chapters.

2.3.1 Microwave plasma atomic emission spectroscopy (MP-AES)

Atomic emission spectrometry (AES) is the technique of exciting atoms for determining elemental composition and concentration of a sample. It involves exciting an atom of a sample using an external energy source [93]. When this atom falls back to its ground state, it emits a characteristic wavelength. The different atoms of the samples will provide an overall characteristic pattern of wavelength emission, and higher concentrations of atoms found in a sample will generate higher intensity emissions.

Microwave Plasma atomic emission spectroscopy (MPAES) is a form of AES but is characterized by the energy source it uses to excite the sample atoms. It uses microwave energy to create a plasma discharge from a nitrogen source, as illustrated in figure 2.6 [94]. The plasma goes on to interact with the sample atoms, which are in a nebulized state. The emissions of the atoms are then registered in a detector and its intensities are measured.

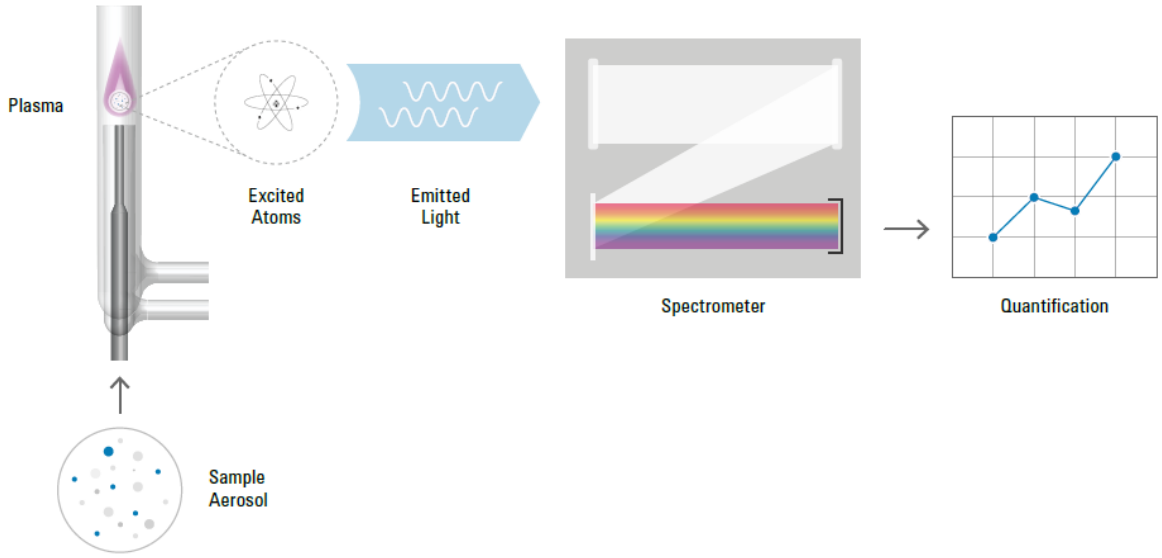

Figure 2.4. Sample aerosol interaction with plasma causing excited atoms generated characteristic light emissions, which are then quantified [94].

For this study, Agilent 4100 MP-AES was used. The parameters are specified as the following. The nebulizer pressure was 180 kPa, optimized for each element. A double-pass glass cyclonic spray chamber was used to spray the plasma onto the sample, and quartz torch was used to induce the plasma. Acquisition parameters include sample uptake delay of 15 seconds, stabilization time of 17 seconds, read time of 3 seconds.

2.3.2 Scanning electron microscopy with energy dispersive spectroscopy (SEM-EDS)

Electron microscopy is a broad category of analysis method used to examine, document and analyze materials and its components. This category comprises Scanning and Transmission electron microscopies (SEM and TEM), although for the purpose of this research SEM was used. SEM enables simultaneously many modes of analysis including of Secondary electron Imaging (SEI), backscattered electron (BSE) Imaging, and energy dispersive x-ray spectroscopy (EDX and EDS). A simplified drawing showing the basic components of SEM is depicted in figure 2.8 [95].

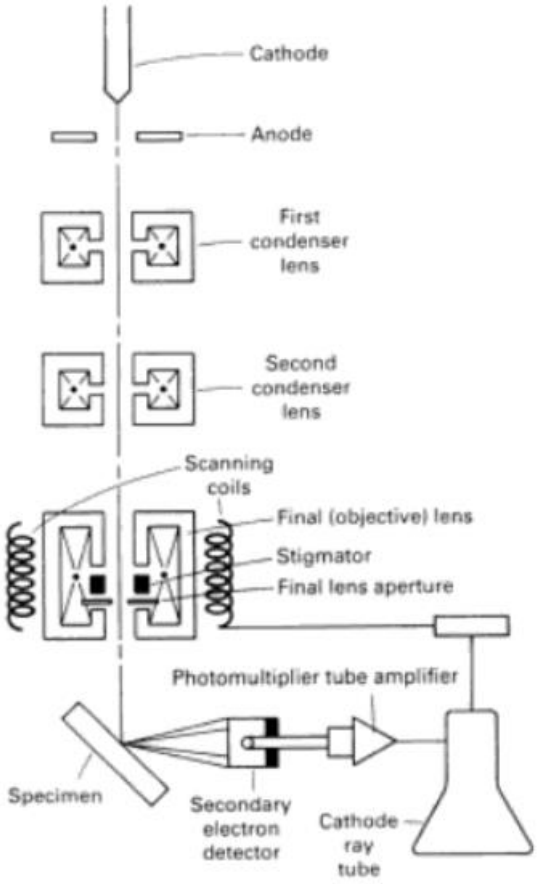

Figure 2.5. Schematic of an SEM system [95].

Overall, an SEM works by heating a cathode tungsten filament, ejecting electrons. The electron beam is accelerated and condensed via an anode and condenser lens, respectively. The electron beam now focused to a small area is incident upon a sample surface and scanned across the sample over an area of interest. The interaction between the incident electron beam and conductive sample generates either secondary electrons at near sample surface depth or backscattered electrons when the depth is larger. These secondary and backscattered electrons are registered by a detector which converts them into signals by converting electron energy into photon energy. These signals give information regarding surface morphology of the sample, which is essentially the function of SEM [96].

During interaction between the incident beam and sample surface, in addition to the secondary and backscattered electron, an additional phenomenon occurs, that is, the production of characteristic x-rays. X-rays are formed when the energy of the incident

electron ejects an inner-shell electron of the sample atom, subsequently causing an outer shell atom to fill the inner-shell vacancy and producing an X-ray photon as a result of the difference in energy between outer and inner shell of the atom. The emitted X-ray photon energies are characteristic of the atom being analysed which is how EDS, a function incorporated into the SEM system, is used to identify atomic composition of samples [96].

For this project, a Tescan VEGA3 scanning electron microscope equipped with EDS (SEM-EDS) was used to perform both non-destructive surface characterization and elemental analysis for localized areas of the sample. The analysis was performed with a working voltage of 10 KV.

2.3.3 X-ray diffraction (XRD)

The principles of XRD are based on the interaction between X-ray photons and electrons surrounding the nuclei of sample atoms. The X-ray photons scattered by the atoms do not change in energy and retain the phase relationship to the incident wave [97]. The sample being analyzed in an XRD is a crystalline structure of periodic nature, resulting in constructive or destructive scattered photons. These phenomena can be best explained along with Bragg's law form the basis of XRD. Bragg's law may be best explained by referring to the figure 2.8 [98].

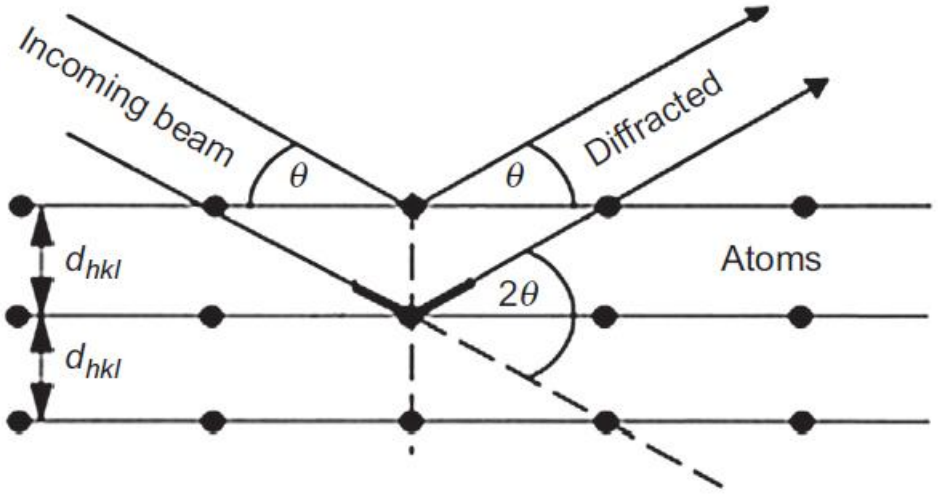

Figure 2.6. Bragg scattering from a set of crystal planes with spacing d_{hkl}.

The Bragg's law is based on the diffraction of X-ray on the atomic plane and the angle of the diffracted signal, and is given in the equation 2.3 below:

$$n\lambda = 2d_{hkl}sin(\theta) \quad \text{Eq. 2.3}$$

Where λ represents the wavelength of the incident beam, in nm, d_{hkl} represents the lattice spacing in nm, and θ being the angle of the incident beam. In a typical test, the angle of the beam is varied and accordingly the intensity of the diffracted signal is recorded for each angle.

In this study, X-ray diffraction was performed using PANalytical Aeris model FB705 to evaluate the composition of anode layer before and after galvanostatic test. The incoming x-ray beam source were Cu-Kα with wavelength λ=0.154 nm. We employed powder preparation where the samples were loaded on Zero Background holders. The results were collected for 2θ between 15° and 70°, step size of 0.022° and scan step time of 23.97 seconds. The data were interpreted using Highscore software.

2.3.4 X-ray fluorescence (XRF)

X-ray Fluorescence (XRF) was used in this project to determine the concentration of manganese deposition on the anode surface during the linear sweep voltammetry. XRF uses incident X-rays as a mode to strike sample atoms dislodging the inner orbital of atom the atom. The atom regains stability by filling the vacancy left in the inner orbital shell with an electron from one of the atom's higher energy orbital shells. The energy difference between higher and lower orbital results in the release of a fluorescent X-ray, which is characteristic of the sample atom [99]. The machine used was a Rigaku ZSX Primus, which makes semi-quantitative or quantitative determination of minor and major atomic elements in a variety of sample types.

Chapter 3: Results and discussion

3.1 Developing filtering and sampling method

After each electrolysis test, especially galvanostatic tests, the electrolyte solution has some solid particles such as manganese oxide and lead oxide which are suspended or precipitated. To take a sample from electrolyte and analyse with the Microwave Plasma Atomic Emission spectroscopy (MP-AES) analyser, the samples must be transparent and without any solid particles.

To find the best method to filter the samples, a series of methods were carried out after 2 h of galvanostatic test. The conditions of the electrolyte were including 55 g L^{-1} Zn^{2+}, 1 g L^{-1} Mn^{2+}, pH 1, temperature 40 °C and current density 500 A m^{-2}.

In the first method, the samples (samples 1 – 6) were taken from the electrolyte and kept in tubes. They were allowed to naturally precipitate the oxide particles. Also, to investigate the effect of HNO_3 on the samples and to obtain a clear sample, HNO_3 5 % was added to these samples. HNO_3 5 % is the dilution solution to use MP-AES analyser.

In other methods, samples (samples 7 – 11) were filtered, using alumina wool and syringe filter (basix NYL 0.45 μm sterile) under different conditions including applying pressure with the piston and using centrifuge. For using the centrifuge, the samples were kept in the refrigerator for one day to keep them in low temperature. Moreover, the samples were in the centrifuge for one hour at 1520 rpm.

All these methods were applied to make sure that no MnO_2 particle remains in suspension to interfere with the results and to get accurate concentration of Mn ions in the electrolyte. The MnO_2 particles in suspension are considered as the “oxidized” Mn, thus should be removed properly from the electrolyte before MP analysis. The filtered samples were examined visually. Table 3.1 presents the results of filtration method.

Table 3.1. Filtration method and their results.

Name of samples	Filtration Method	Conditions	Results
1	No filter	After 1 h precipitation	Not clear
2	No filter	After 1 h precipitation and adding HNO_3 5%	Not clear
3	No filter	After 2 h precipitation	Not clear
4	No filter	After 2 h precipitation and adding HNO_3 5%	Not clear
5	No filter	After 3 h precipitation	Not clear
6	No filter	After 3 h precipitation and adding HNO_3 5%	Not clear
7	Alumina wool	With pressure	Clear
8	Alumina wool	Without pressure	Clear
9	Syringe	With pressure	Clear
10	Alumina wool	With pressure and using centrifuge and low temperature	Clear
11	Syringe	With pressure and using centrifuge and low temperature	Clear

To find the best filtration method corresponding to the results, time and cost, filtration with alumina wool was chosen and all remaining samples were filtered using this method.

In all galvanostatic tests, the samples were taken at 0 min, 30 min, 60 min, 90 min and 120 min. Figure 3.1 shows the samples at each 30 min which are filtered by alumina wool filtration method.

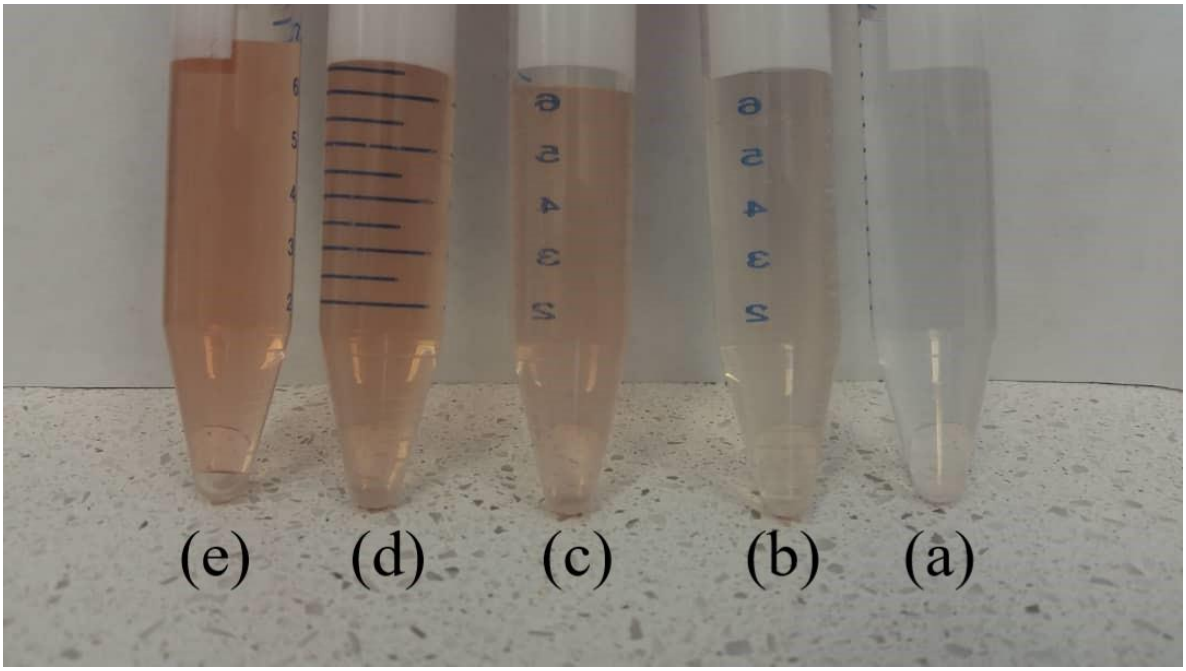

Figure 3.1. samples of galvanostatic tests after a) 0 min, b) 30 min, c) 60 min, d) 90 min and e) 120 min of electrolysis.

3.2 Galvanostatic tests

The galvanostatic tests were carried out for 2 h in both purification and electrowinning conditions to find optimum conditions for manganese removal. In these series of tests, anodic voltages of each test were recorded by DataTaker and current efficiency was calculated based on equation 2.1. Figures 3.2 and 3.3 show the effect of current density and temperature on current efficiency, respectively, for two electrowinning conditions.

In order to have the reliable data, each galvanostatic tests was repeated for the minimum of 3 times. To present the results of these series of test, the averages of the current densities were used. The average and standard deviation of calculation for the current efficiencies in both electrowinning and purification conditions were plotted in the figures 3.2, 3.3, 3.8 and 3.10.

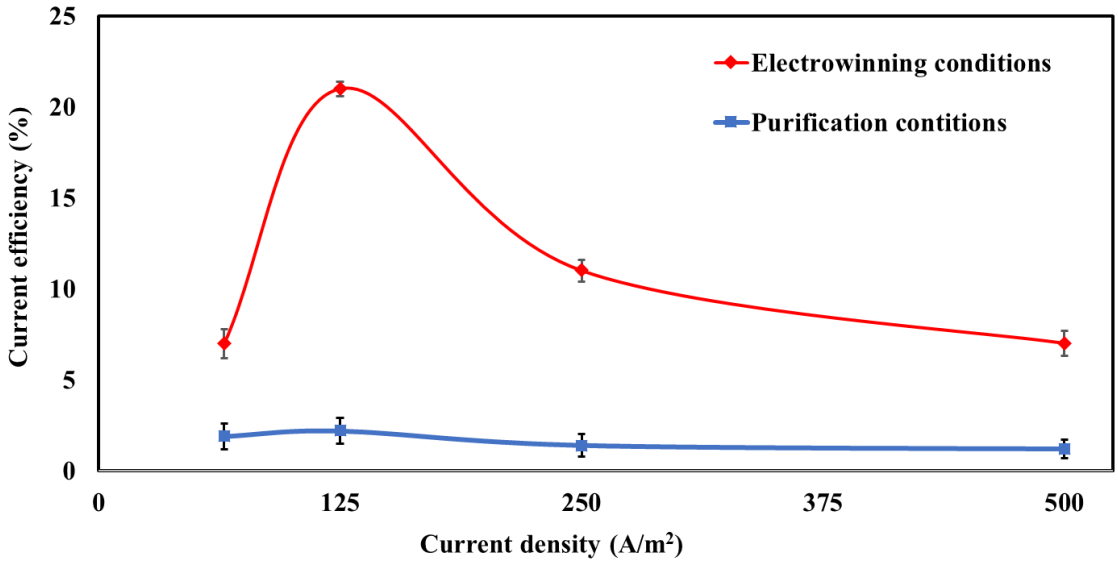

Figure 3.2. The current efficiency of Mn removal as a function of current density for standard electrowinning electrolytes: 55 g L^{-1} Zn^{2+}, 252 g L^{-1} H_2SO_4 and l g L^{-1} Mn^{2+} and standard purification electrolytes: 150 g L^{-1} Zn^{2+}, l g L^{-1} Mn^{2+}, pH 4. Total duration of experiment was 2 h.

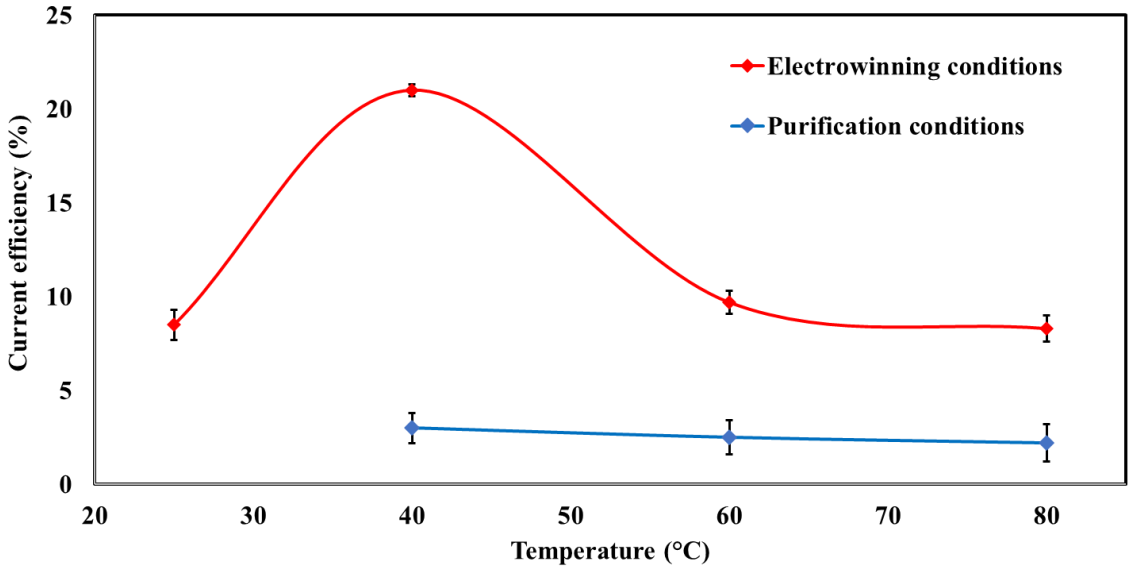

Figure 3.3. The current efficiency of Mn removal as a function of temperature for standard electrowinning electrolytes: 55 g L^{-1} Zn^{2+}, 252 g L^{-1} H_2SO_4 and l g L^{-1} Mn^{2+} and standard purification electrolytes: 150 g L^{-1} Zn^{2+}, l g L^{-1} Mn^{2+}, pH 4. Total duration of experiment was 2 h.

According to these results, for both electrowinning and purification conditions, the highest current efficiency for manganese removal was obtained at 125 A m^{-2} (Fig. 3.2) at 40 °C (Fig. 3.3). The current efficiency values in electrowinning condition were much higher than those in purification condition. The highest current efficiency value for manganese dioxide formation, with an initial concentration of 1 g L^{-1} of Mn^{2+}, was 21 % which was obtained in electrowinning condition after 2 h of electrolysis. The highest current efficiency value in purification condition was 2 % after the same time.

Figures 3.4, 3.5, 3.6 and 3.7 present the effect of current density in electrowinning conditions on anodic voltage, the effect of current density in purification conditions on anodic voltage, the effect of temperature in electrowinning conditions on anodic voltage and the effect of temperature in purification conditions on anodic voltage, respectively. The recorded anodic voltages of these tests in both electrowinning and purification conditions show that the anode potential increased when the current density increased (Figs. 3.4 and 3.5) and the temperature decreased (Figs. 3.6 and 3.7). However, increasing the temperature evolves the oxygen in lower potential on the anode and this reaction prevents the deposition of manganese on the anode [100]. In conclusion, current efficiency of manganese deposition decreases when temperature increases.

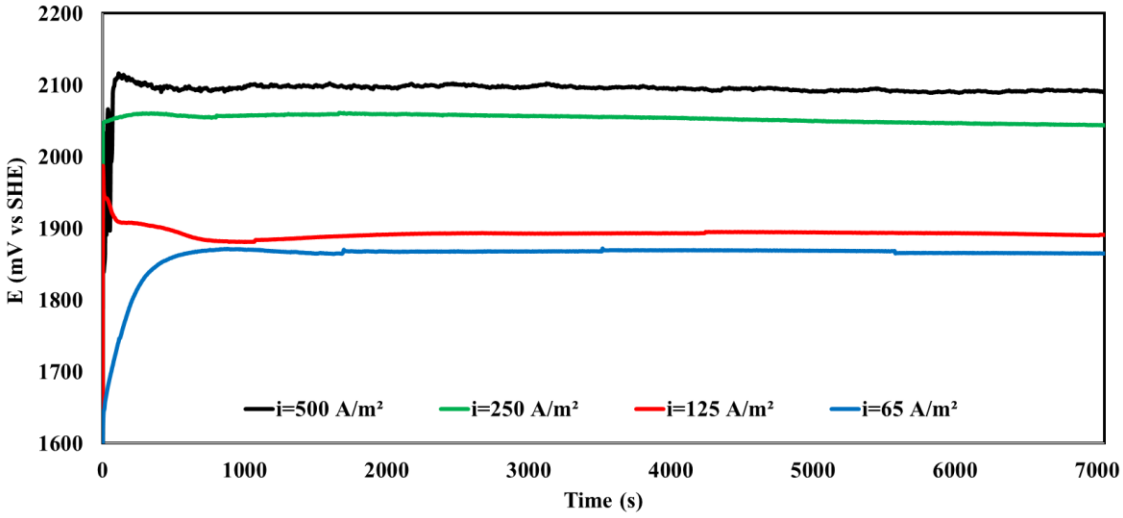

Figure 3.4. Effect of current density in electrowinning conditions on anodic voltage. Electrolyte compositions include: 55 g L^{-1} Zn^{2+}, 252 g L^{-1} H_2SO_4 and l g L^{-1} Mn^{2+}.

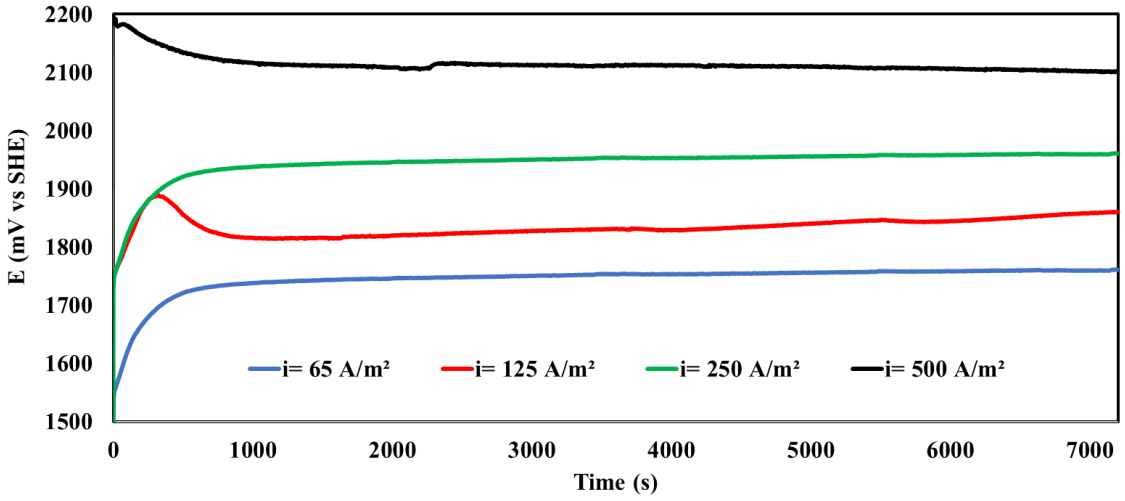

Figure 3.5. Effect of current density in purification conditions on anodic voltage. Electrolyte compositions include: 150 g L^{-1} Zn^{2+}, l g L^{-1} Mn^{2+} and pH 4.

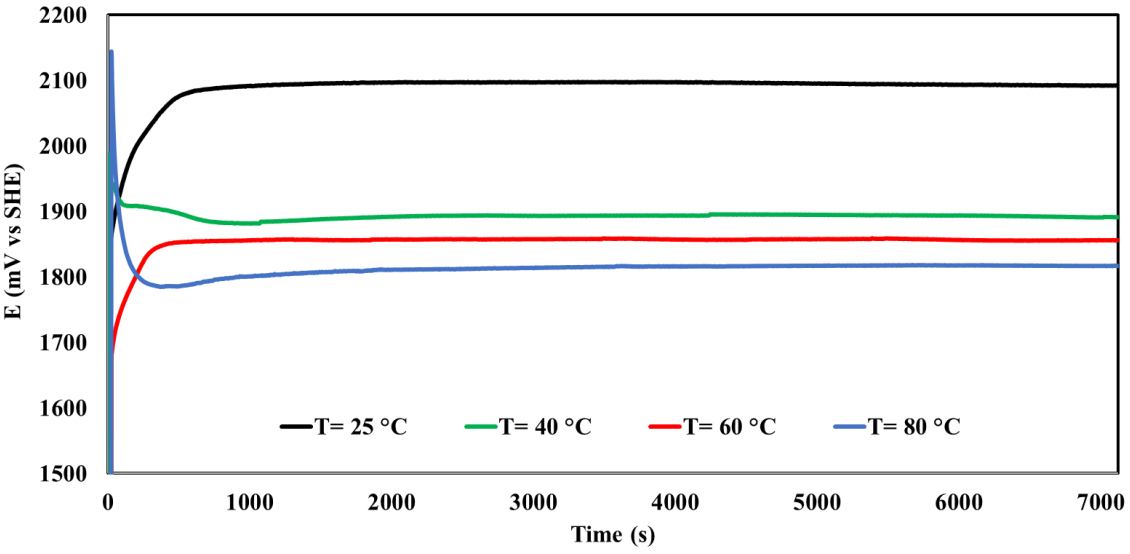

Figure 3.6. Effect of temperature in electrowinning conditions on anodic voltage. Electrolyte compositions include: 55 g L^{-1} Zn^{2+}, 252 g L^{-1} H_2SO_4 and l g L^{-1} Mn^{2+}.

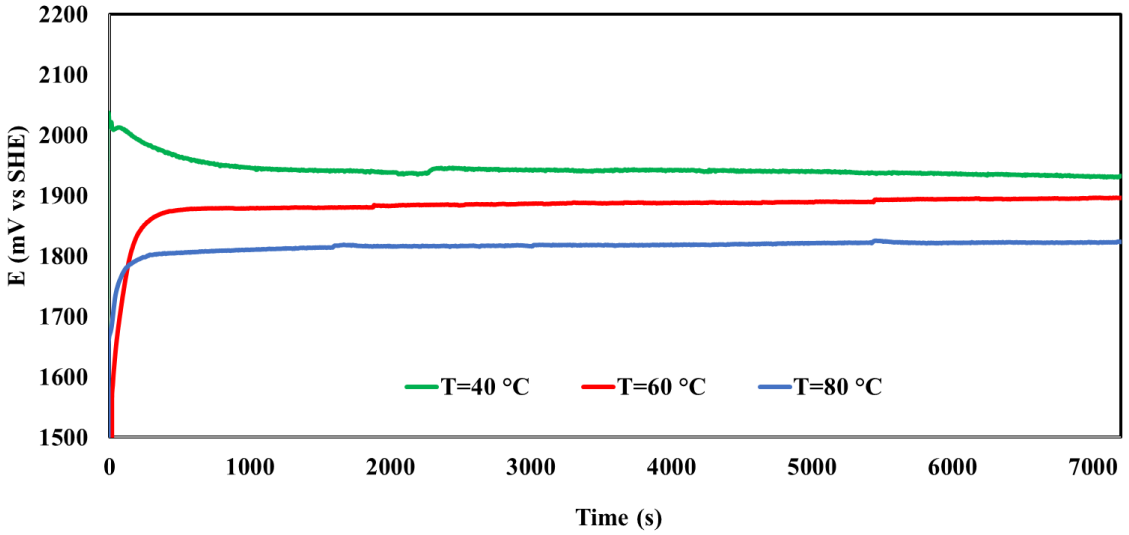

Figure 3.7. Effect of temperature in purification conditions on anodic voltage. Electrolyte compositions include: 150 g L^{-1} Zn^{2+}, l g L^{-1} Mn^{2+} and pH 4.

After finding the best current density and temperature for manganese removal, to investigate the effect of pH on current efficiency of manganese removal, a test was carried out for 2 h with these conditions: 55 g L^{-1} Zn^{2+}, l g L^{-1} Mn^{2+} and pH 4. In other words, this test was carried out in the optimum current density and temperature for manganese removal as pervious results but at pH 4. Figure 3.8 presents the effect of pH on current efficiency of manganese removal at two different pH. Also, figure 3.9 shows the effect of pH on the anodic voltage in the previous conditions.

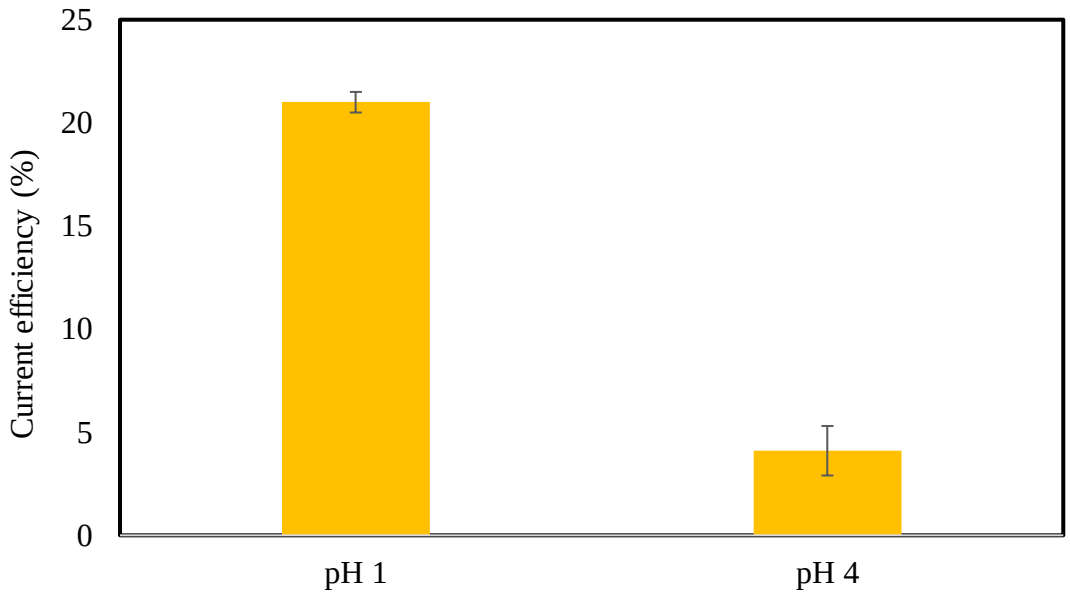

Figure 3.8. Effect of pH on current efficiency of manganese removal. Electrolyte conditions: temperature 40 °C, current density 125 A m^{-2}, 55 g L^{-1} Zn^{2+} and l g L^{-1} Mn^{2+}.

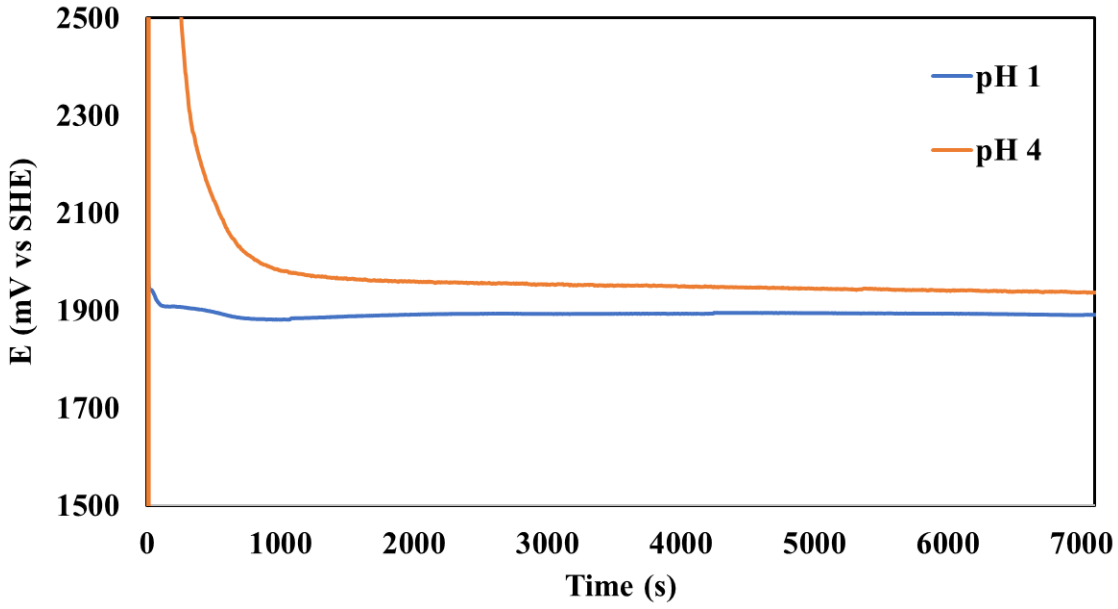

Figure 3.9. Effect of pH on anodic voltage. Electrolyte conditions: temperature 40 °C, current density 125 A m^{-2}, 55 g L^{-1} Zn^{2+} and l g L^{-1} Mn^{2+}.

It can be observed that by increasing pH from 1 to 4, current efficiency significantly decreases, while the anodic voltage decreases drastically in the first 1000 s and then stays higher (between 50-100 mV) during the rest of experiment.

In order to investigate the effect of manganese concentration on current efficiency of manganese deposition, further tests in the best operating conditions obtained above, i.e., at 40 °C and at a current density of 125 A m^{-2}, were carried out. The current efficiency was calculated at the end of 2 h of galvanostatic tests, for each Mn^{2+} concentration. Figure 3.10 shows the current efficiency as a function of initial Mn^{2+} concentration in the solution.

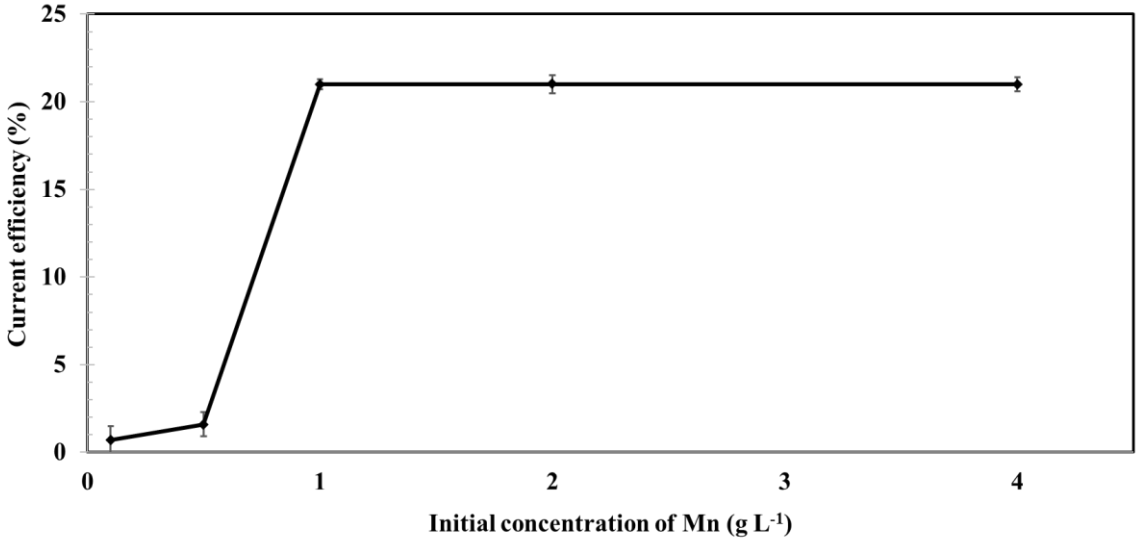

Figure 3.10. The current efficiency obtained for various concentrations of Mn^{2+} in the electrolyte including 55 g L^{-1} Zn^{2+}, 252 g L^{-1} H_2SO_4 at 40 °C and at 125 A m^{-2} after 2 h of electrolysis.

For Mn^{2+} concentrations up to 0.5 g L^{-1}, the current efficiency was low (less than 2 %). Then it increased quickly when the Mn^{2+} concentration increased to 1 g L^{-1}. Further increase in Mn^{2+} concentration did not change the current efficiency. This behaviour indicates that the Mn oxidation rate is primarily governed by diffusion at low concentrations. When the concentration is lower than 1 g L^{-1}, a lack of Mn^{2+} ion mass transfer towards anode surface can be created. At higher concentrations, diffusion is conducted quite well and the Mn deposition is governed by the surface reaction kinetics. Furthermore, the current efficiency stayed constant beyond the concentration of 1 g L^{-1}.

To obtain the CE at different time intervals (instead of calculating it at the end of 2 h period), the cumulative current efficiency is presented as a function of time for different manganese concentrations (Figure 3.11). For this series of tests, the fresh lead-silver anodes were used at the beginning of each electrolysis and they were not cleaned in the time intervals. The results showed that at lower manganese concentrations (0.1 to 0.5 g L^{-1}), the cumulative current efficiency stays quasi-constant during 120 min of electrolysis time. However, for Mn^{2+} concentrations higher than 1 g L^{-1} the cumulative CE decreased significantly during first hour of electrolysis and then continued to decrease with lower rate till the end of the second hour. The current efficiency for each interval of 30 min was also calculated independently, revealing that it is around 32 % for the first interval and about 11 % for the last interval. This strongly suggests that the cleanliness of surface can considerably influence the CE of manganese removal.

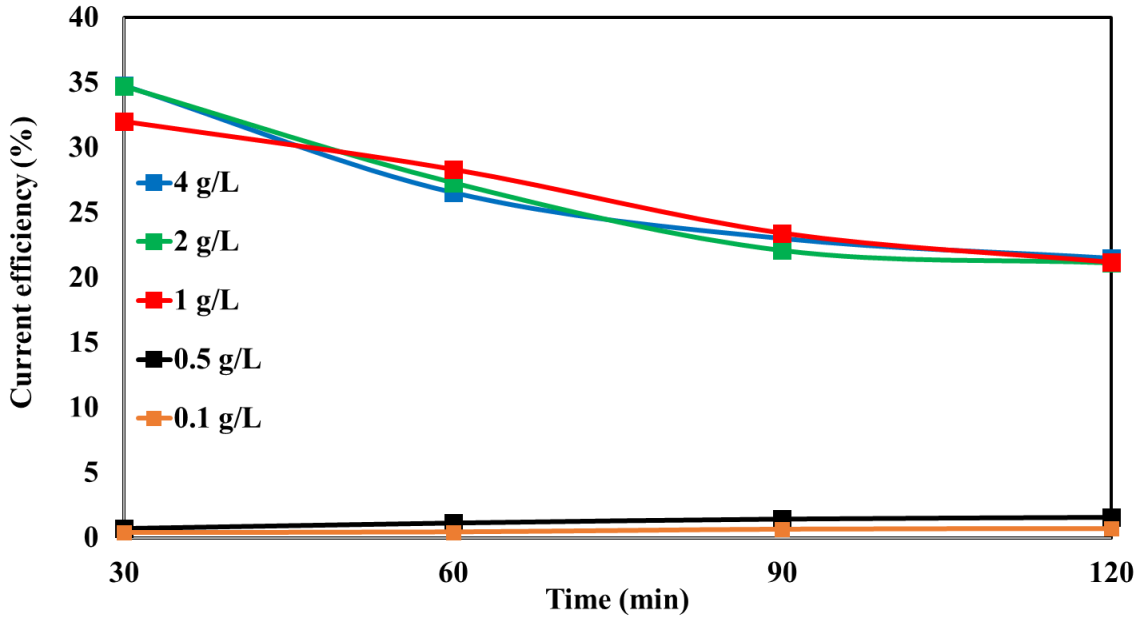

Figure 3.11. Accumulative current efficiency obtained for various concentrations of Mn^{2+} in the electrolyte including 55 g L^{-1} Zn^{2+}, 252 g L^{-1} H_2SO_4 at 40 °C under 125 A m^{-2} after 30, 60, 90 and 120 min of electrolysis.

In order to investigate the effect of anode surface cleanliness on the current efficiency and concentration of manganese in the electrolyte over time, following test was carried out. The used Pb-Ag anode was replaced by fresh anode after each 30 min during the test. To make the fresh anode, the surface of anode was polished to remove all the oxides and other impurities. The obtained manganese concentrations, current efficiency and recorded anodic voltage of this test, are presented in figures 3.12, 3.13 and 3.14, respectively. Also, the results of this test were compared with the results of best conditions for manganese removal which obtained before.

It can be clearly observed that concentration of manganese in the electrolyte decreases much faster for the performed test with fresh anode. Also, the slight decrease of current efficiency in the test with fresh anode from 31 % at the first interval to 28 % at the last interval is attributed to fact that the concentration of Mn^{2+} decreases also from 1 g L^{-1} to about 0.5 g L^{-1}, respectively for these intervals. Thus, the decrease of the Mn^{2+} concentration influences the diffusion rate, slightly reducing the current efficiency.

Furthermore, figure 3.14 shows that anodic voltage in the test with fresh anode is remain at the same potential after each 30 min of cleaning. Also, the potential of anode in this test is higher than the potential of anode in the test without cleaning of anode. Higher anodic potential evolves the oxygen in higher potential on the anode and this reaction improves the deposition of manganese on the anode. In conclusion, by using the fresh anode, manganese deposition and current efficiency increased.

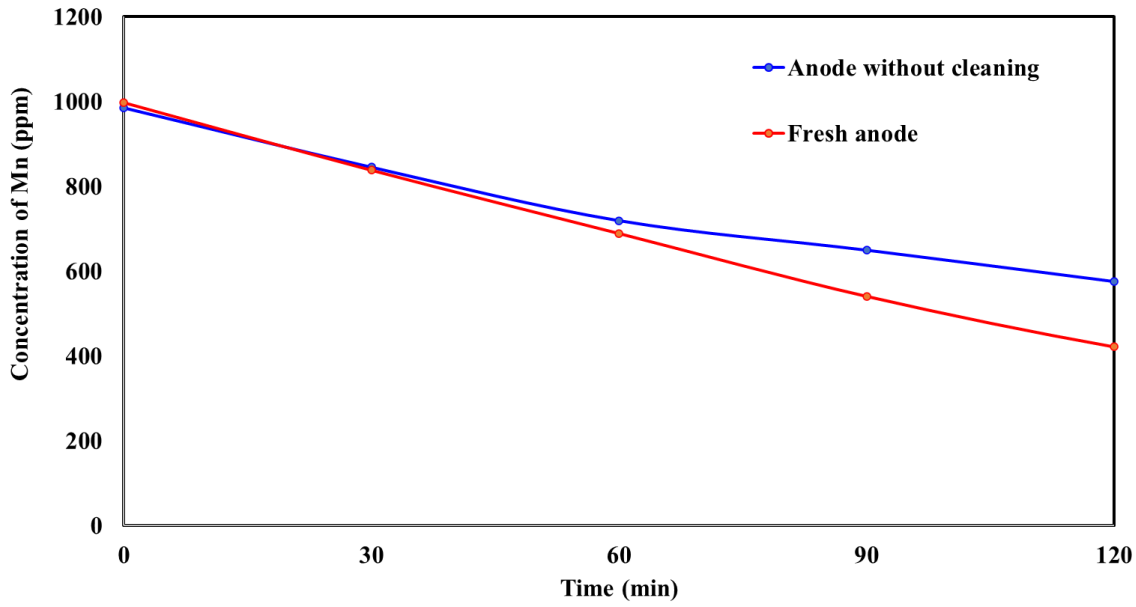

Figure 3.12. Cumulative manganese concentration obtained by MP-AES analyser for 1 g L^{-1} Mn^{2+} concentration in the electrolyte including 55 g L^{-1} Zn^{2+}, 252 g L^{-1} H_2SO_4 at 40 °C and 125 A m^{-2} after 30, 60, 90 and 120 min of electrolysis.

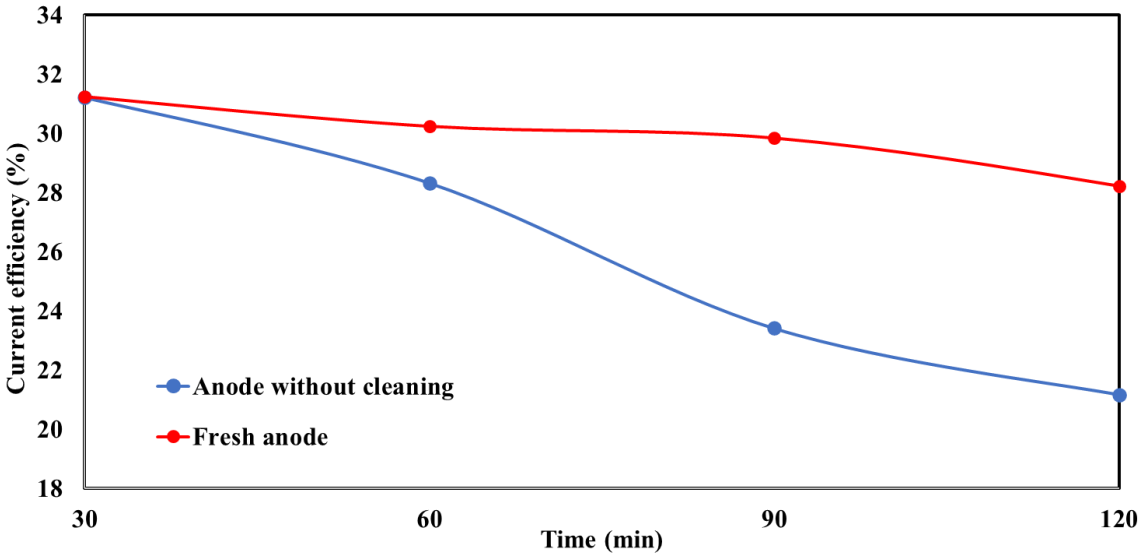

Figure 3.13. Cumulative current efficiency calculated for 1 g L^{-1} Mn^{2+} concentration in the electrolyte including 55 g L^{-1} Zn^{2+}, 252 g L^{-1} H_2SO_4 at 40 °C and 125 A m^{-2} after 30, 60, 90 and 120 min of electrolysis.

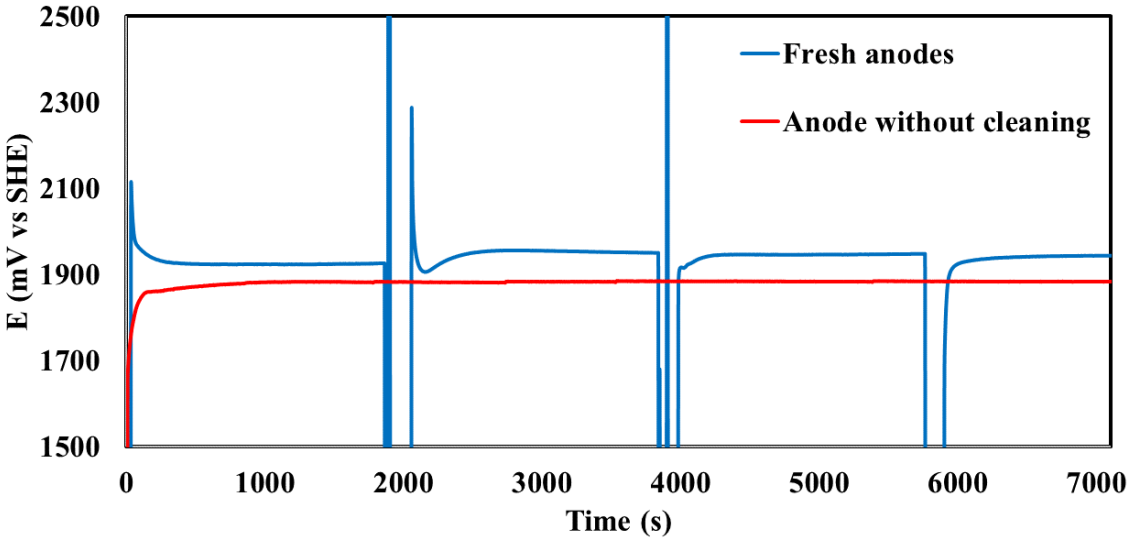

Figure 3.14. Cumulative anodic voltage recorded for 1 g L^{-1} Mn^{2+} concentration in the electrolyte including 55 g L^{-1} Zn^{2+}, 252 g L^{-1} H_2SO_4 at 40 °C and 125 A m^{-2} after 30, 60, 90 and 120 min of electrolysis.

In this research, current efficiency of zinc deposition as a part of reactions in the electrolyte cell was studied. The current efficiencies of zinc deposition were calculated based on equation 2.1 for different galvanostatic tests in electrowinning operation conditions. To obtain the actual weigh of zinc deposition, zinc deposited on the cathode was gently removed and weighed using balance. These tests were carried out in different temperatures including 25, 40, 60 and 80 °C (table 3.2). Also, to accumulate current efficiency of manganese deposition and zinc deposition, two current density were applied: 125 A m^{-2} (best current efficiency for manganese removal) and 500 A m^{-2} (optimum current density in industrial for zinc deposition). Table 3.3 and figure 3.15 present effect of current density on current efficiency and cathodic voltage, respectively. The electrolytes composition used for these tests include 55 g L^{-1} Zn^{2+}, 1 g L^{-1} Mn, 252 g L^{-1} H_2SO_4 (pH 1) and tests were carried for 2 h of electrolysis.

According to the results, current efficiency of cathodic zinc deposition increases when temperature and current density increase, while current efficiency of anodic manganese deposition increases when temperature and current density decrease.

Moreover, by increasing the current density, cathodic voltage is decreased which reduce hydrogen overpotential and improve the zinc deposition on the cathode [45] (figure 3.15).

Table 3.2. Effect of temperature on current efficiency of zinc deposition at current density of 125 A m^{-2}.

Temperature (°C)	**25**	**40**	**60**	**80**
Current efficiency of zinc deposition (%)	82	84	88	90

Table 3.3. Effect of current density on current efficiency of zinc deposition at 80 °C.

Current density (A m^{-2})	**125**	**500**
Current efficiency of zinc deposition (%)	90	97

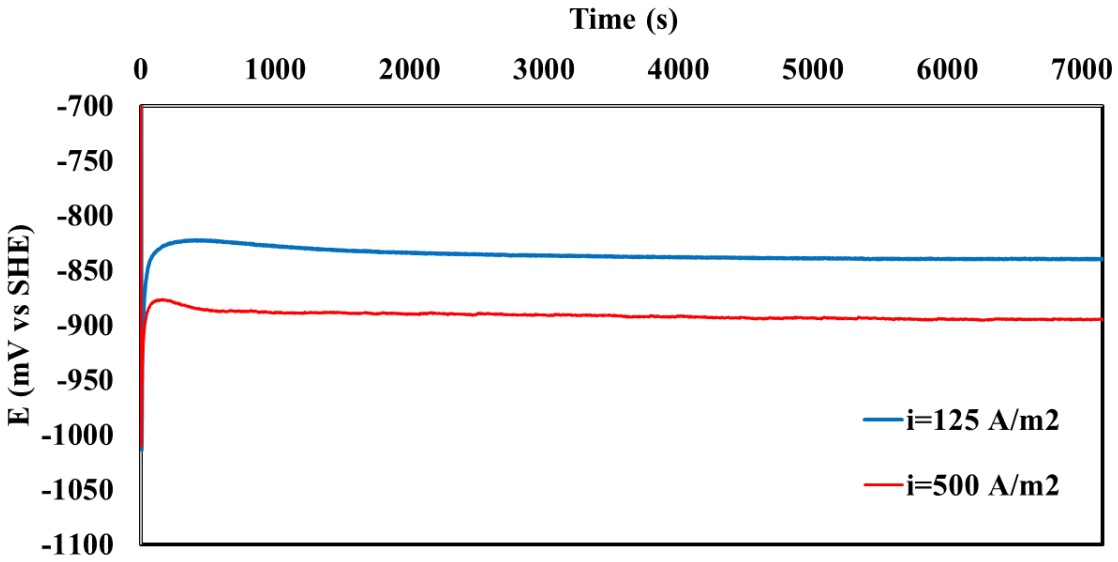

Figure 3. 15. Effect of current density on cathodic voltage of zinc deposition at 80 °C.

3.3 Linear sweep voltammetry (LSV)

The effect of temperature and Mn^{2+} concentrations on the oxygen evolution reaction (OER) on Pb-0.7%Ag anode was studied in the zinc sulfate electrolyte. The effect of three temperatures 40, 60 and 80 °C on anodic polarization curves on the surface of a fresh lead-silver anode are shown in Fig. 3.16.

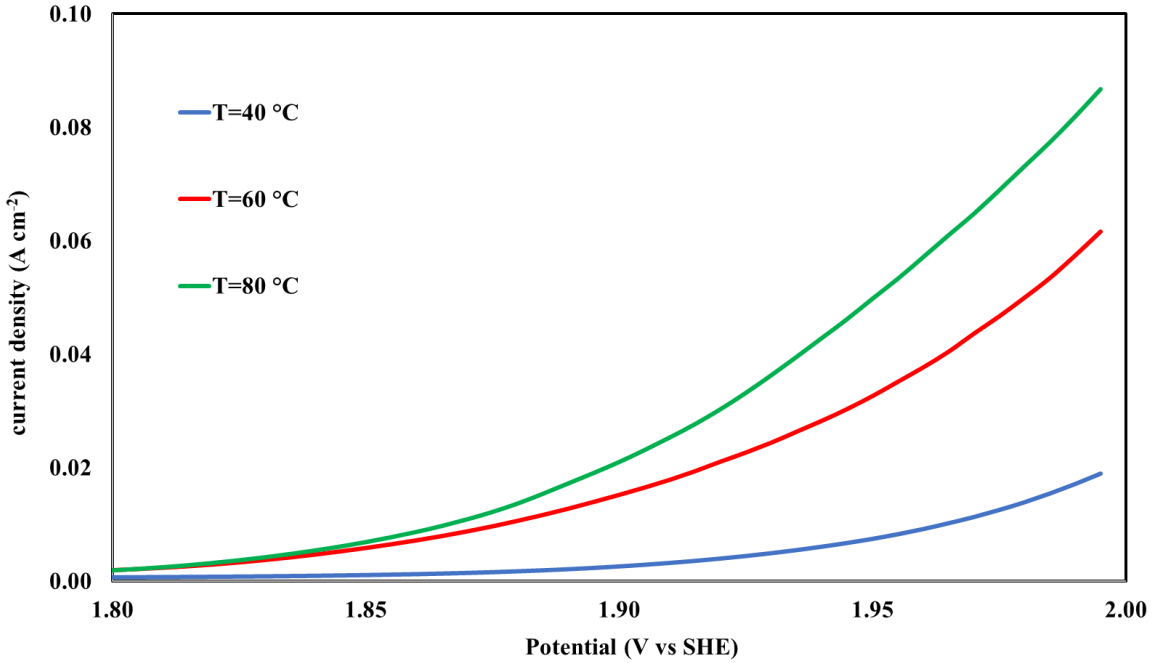

Figure 3.16. LSV curves obtained in the electrolyte including 55 g L^{-1} Zn^{2+}, 252 g L^{-1} H_2SO_4, 1 g L^{-1} Mn^{2+} at 40, 60 and 80 °C.

The increase of temperature was positively affected the OER and depolarized this reaction. These results are in accordance with the results obtained by Zhang *et al.* [2018] [101]. These authors observed the similar tendency for a fresh lead-based anode in zinc sulfate electrolyte without manganese in the range of 20 up to 50 °C. They calculated the exchange current density (j_0) values for OER and drew the Arrhenius plot according to the results and showed that with the increase of temperature, the values of log(j_0) decrease and consequently the oxygen evolution reaction is promoted.

The polarization measurements were carried out in the absence of manganese and in the presence of various manganese concentrations 0.1, 0.5, 1, 2 and 4 g L^{-1} in electrowinning

electrolyte at 40 °C. For better observation of MnO_2 formation peak on polarization curves, the sequence tests with several LSV runs were recorded till reaching a stable curve. Figures 3.17 to 3.22 present the 20 LSV curves for fresh lead-silver anode at manganese concentration 0, 0.1, 0.5, 1, 2, and 4 g L^{-1}. Also, the comparison results are shown in Figure 3.23.

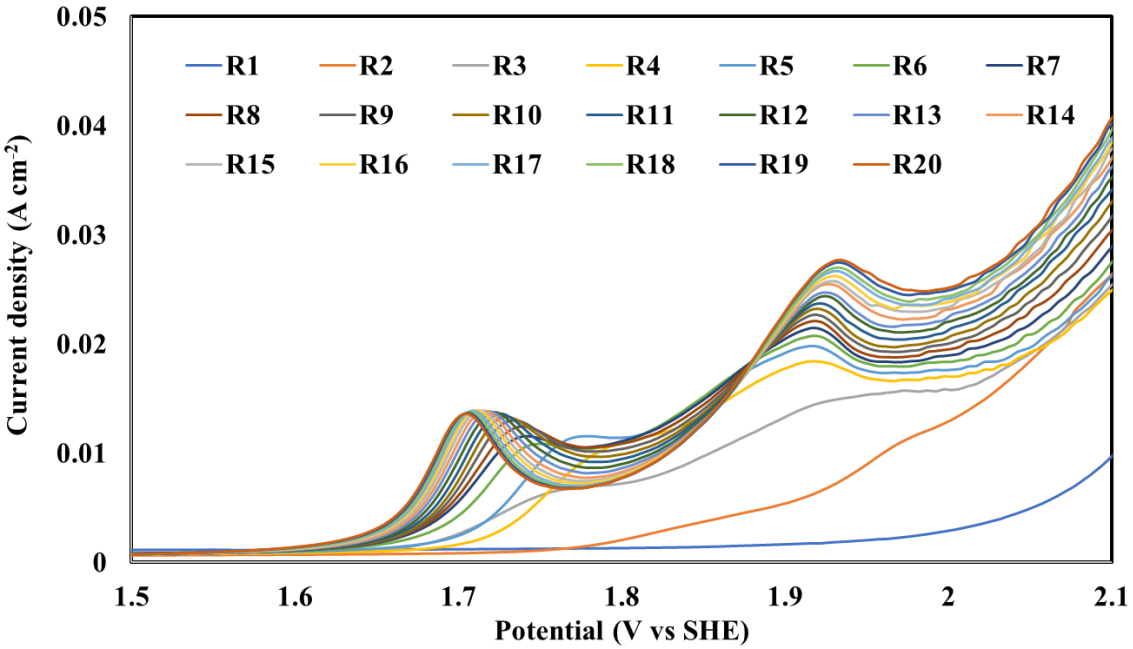

Figure 3.17. LSV curves obtained in the electrolyte including 55 g L^{-1} Zn^{2+}, 252 g L^{-1} H_2SO_4 and without presence of Mn^{2+} at 40°C.

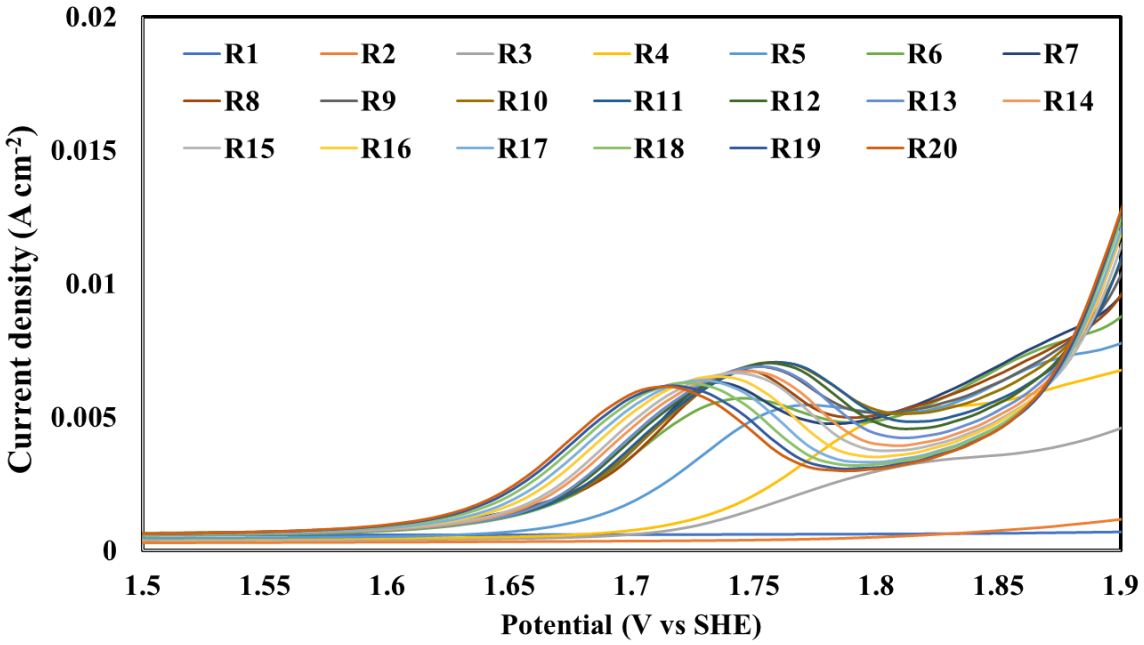

Figure 3.18. LSV curves obtained in the electrolyte including 55 g L^{-1} Zn^{2+}, 252 g L^{-1} H_2SO_4 and 0.1 g L^{-1} Mn^{2+} at 40°C.

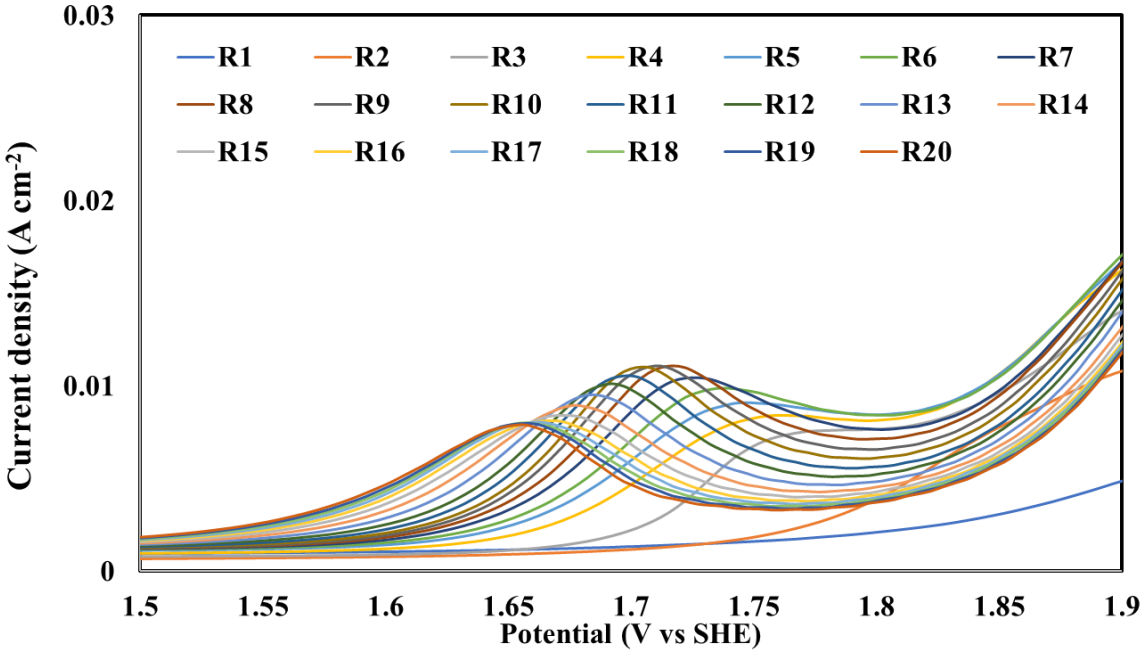

Figure 3.19. LSV curves obtained in the electrolyte including 55 g L^{-1} Zn^{2+}, 252 g L^{-1} H_2SO_4 and 0.5 g L^{-1} Mn^{2+} at 40°C.

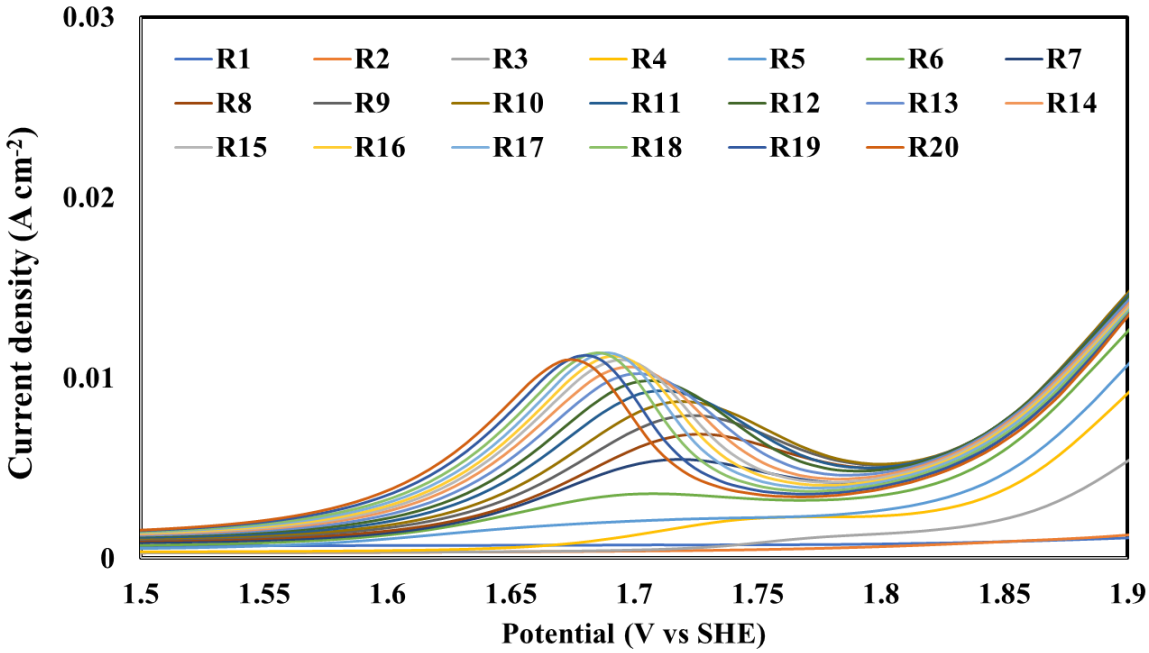

Figure 3.20. LSV curves obtained in the electrolyte including 55 g L^{-1} Zn^{2+}, 252 g L^{-1} H_2SO_4 and 1 g L^{-1} Mn^{2+} at 40°C.

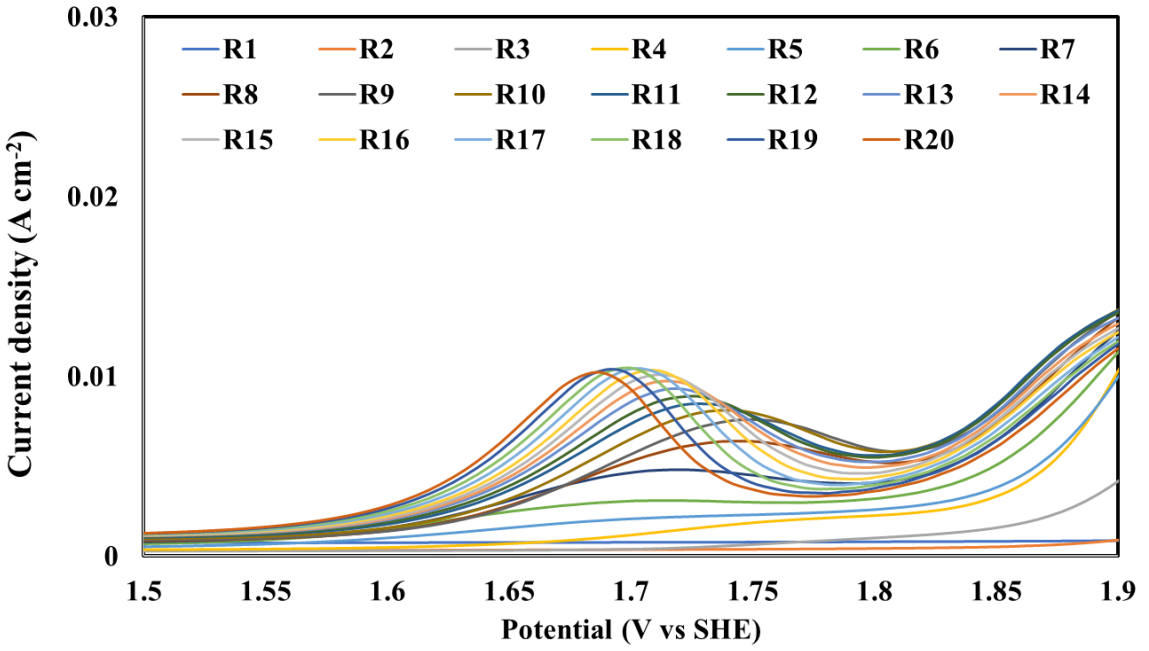

Figure 3.21. LSV curves obtained in the electrolyte including 55 g L^{-1} Zn^{2+}, 252 g L^{-1} H_2SO_4 and 2 g L^{-1} Mn^{2+} at 40°C.

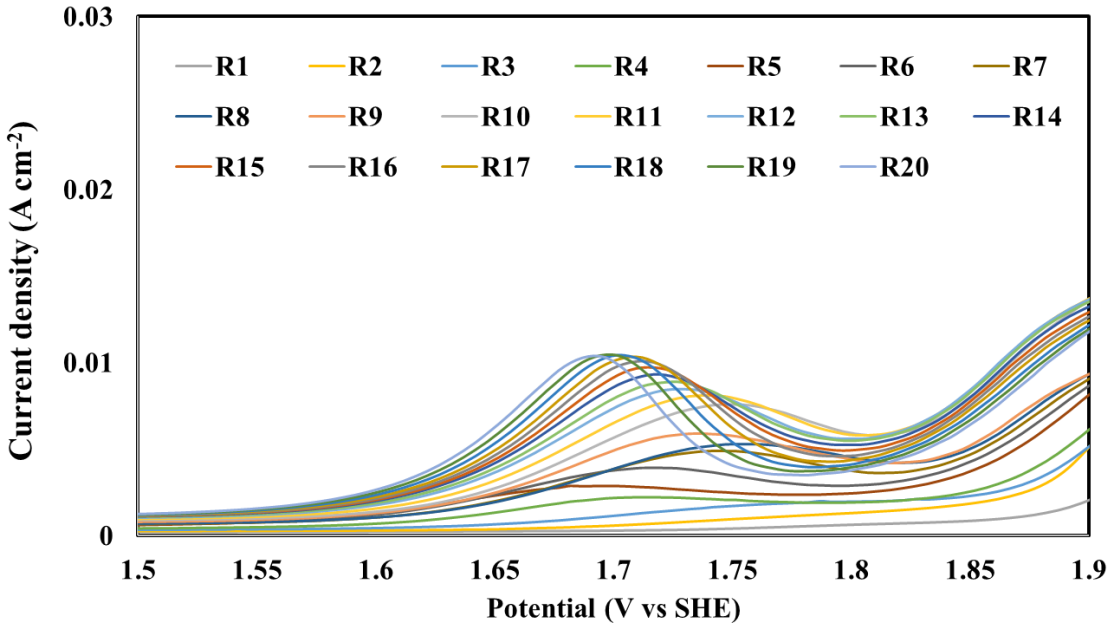

Figure 3.22. LSV curves obtained in the electrolyte including 55 g L^{-1} Zn^{2+}, 252 g L^{-1} H_2SO_4 and 4 g L^{-1} Mn^{2+} at 40°C.

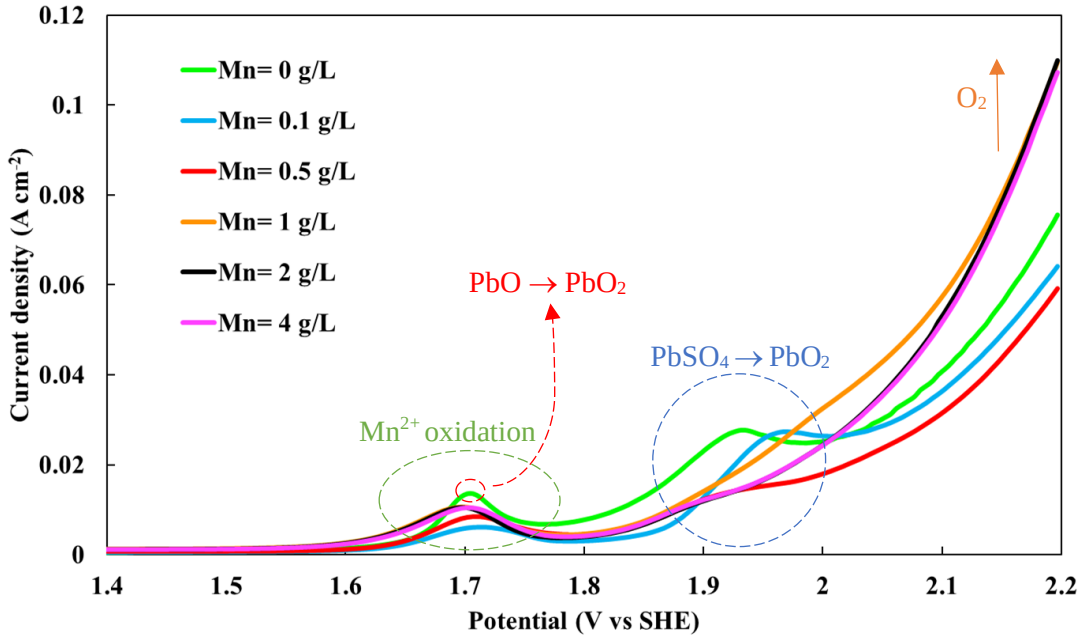

Figure 3.23. LSV curves obtained in the electrolyte including 55 g L^{-1} Zn^{2+}, 252 g L^{-1} H_2SO_4 and various concentrations of Mn^{2+} at 40°C.

The stable LSV curves obtained in different concentrations of manganese were compared together in Figure 3.23. The general LSV curves show the presence of several reactions

happened on the surface of anode electrode. The polarization of Pb-Ag anode in the electrolyte without Mn^{2+} showed the presence of two oxidation peaks due to the corrosion of lead anode followed by oxygen evolution started near 2.0 V. The peak appeared at 1.7 V, could be the oxidation of PbO to *x*PbO.$PbSO_4$ at the inner layer next to the PbO_2 as mentioned by Yu and O'Keefe (2002) [102], or it could also be the oxidation of PbO $\rightarrow$ αPbO_2 close to the surface of anode The second peak observed in the range of 1.85 – 2.0 V is due to the oxidation of $PbSO_4$ to PbO_2 in the outer layer (reaction 3.1).

$$PbSO_4 + 2H_2O \rightarrow PbO_2 + H_2SO_4 + 2H^+ + 2e^- \quad 3.1$$

The oxygen evolution is formed by the dissociation of water according to reaction 3.2.

$$2H_2O \rightarrow O_2 + 4H^+ + 4e^- \quad 3.2$$

In the electrolytes containing different concentrations of manganese, a peak at 1.7 V is clearly observed. This peak is due to the MnO_2 formation according to the following reaction:

$$MnSO_4 + 2H_2O \rightarrow MnO_2 + H_2SO_4 + 2H^+ + 2e^- \quad 3.3$$

The intensity of second peak in the range of 1.85 – 2.0 V decreases with the increase of Mn^{2+} concentration. The reason is that the MnO_2 layer formed on the Pb-Ag surface inhibits more corrosion of Pb and production of PbO_2. For Mn^{2+} concentrations more than 1 g L^{-1}, especially 2 and 4 g L^{-1}, the peak of $PbSO_4 \rightarrow PbO_2$ almost disappeared. The oxygen evolution in the electrolyte including Mn^{2+} progressed easier as compared to the electrolytes without manganese. This confirms the catalytic properties and depolarizing effect of Mn^{2+} ions in the electrolyte during zinc electrowinning [50, 103]. Furthermore, it seems that the concentration of 1 g L^{-1} Mn^{2+} is the saturation limit for diffusion in the electrolyte in our experimental condition since the intensity of MnO_2 peak stayed stable with increasing Mn^{2+} concentration higher than 1 g L^{-1}. This could also be the reason that the current efficiency remains stable at Mn^{2+} concentrations 1, 2 and 4 g L^{-1} (Fig. 3.10).

3.4 Anode surface analysis during LSV tests by XRF

To investigate concentration of manganese and other elements on anode surface and their rate during the LSV tests, the XRF characterization was used. Figure 3.24 presents mass percentage of S, Mn, Ag and Pb on the fresh anode surface (before the tests) and surface of anode during 8 LSV tests. To carry out this analysis, after each round of LSV test, the test was paused, the anode was removed from the electrolyte and the anode surface was analyzed by XRF machine. Then the same anode was used for the next round of LSV test. In all these steps, the surface of the anode was not touched.

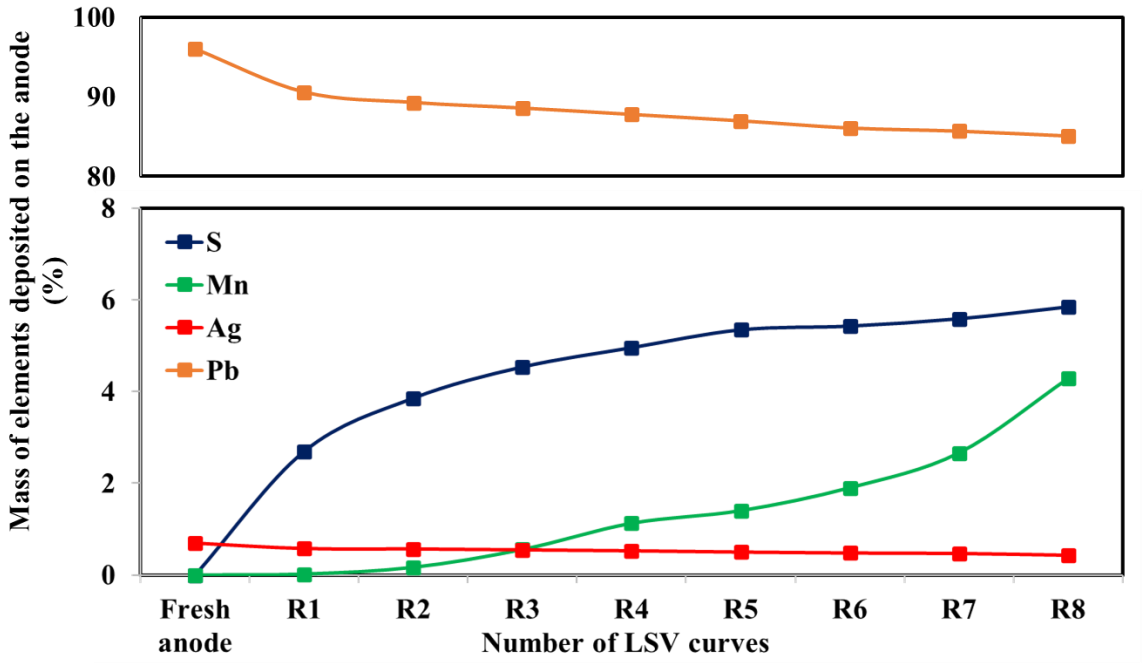

Figure 3.24. XRF analysis on the anode surface during LSV tests.

It can be clearly observed that manganese and sulfur cover the surface of anode during the time. This analysis confirms the mass percentage of silver on the fresh anode which is 0.7 % on the lead anode and the peaks of manganese dioxide formation (Equation 3.3) on the LSV curves which grew up after each round. In the other words, manganese deposited on the anode improves the deposition of manganese.

3.5 SEM characterization of oxide layer after galvanostatic test

The SEM images of microscopic oxide layer on anode surface, after 2 h galvanostatic test, in electrowinning electrolyte, with and without 1 g L^{-1} Mn^{2+} at 40 °C on a fresh anode surface was used for all experiments. Figure 3.25 presents SEM image of fresh Pb-Ag anode. The oxide layer formed on Pb-Ag anode surface in figure 3.26 illustrates a coral-like structure with many cavities and deep holes. According to the EDS analysis, the oxide layer is composed PbO_2 in which the prismatic crystals of $PbSO_4$ around 5 μm in size is distributed on some zones on the surface. In the presence of 1 g L^{-1} Mn^{2+} (figure 3.27), the oxide layer was covered by a large number of layered irregular $PbSO_4$ crystals. The MnO_2 layer is characterized by spherical particles however, sublayer is composed of three different phases of MnO_2, PbO_2 and $PbSO_4$.

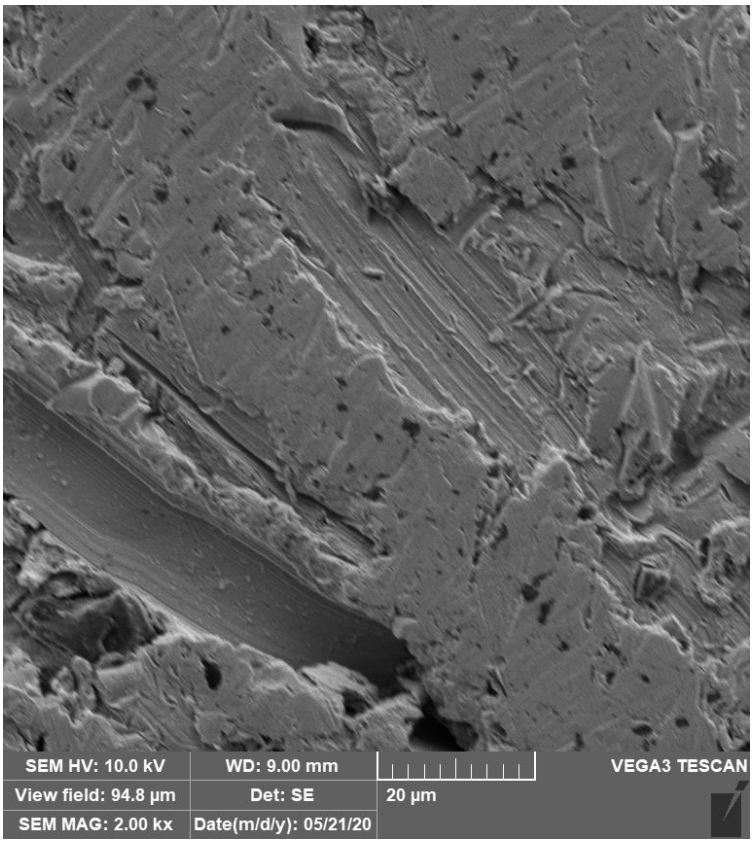

Figure 3.25. SEM micrographs of fresh Pb-Ag anodes.

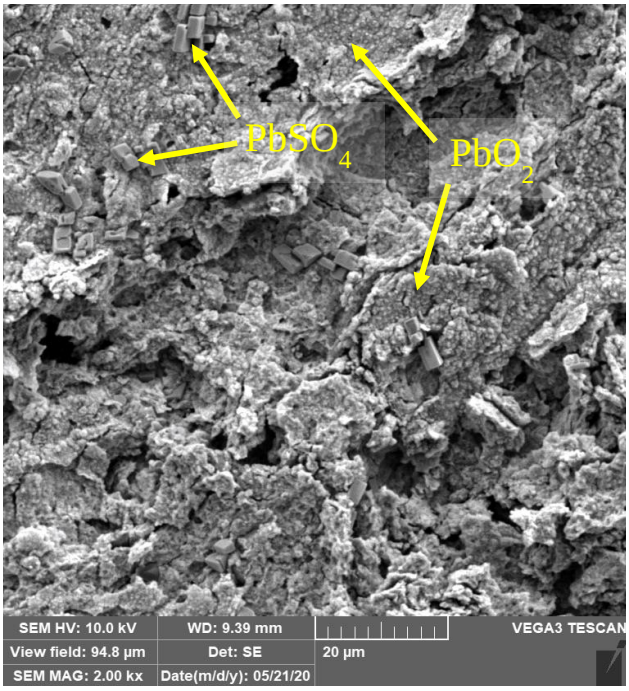

Figure 3.26. SEM micrographs of Pb-Ag anodes after 2 h galvanostatic tests in standard EW solution without manganese at 40 °C.

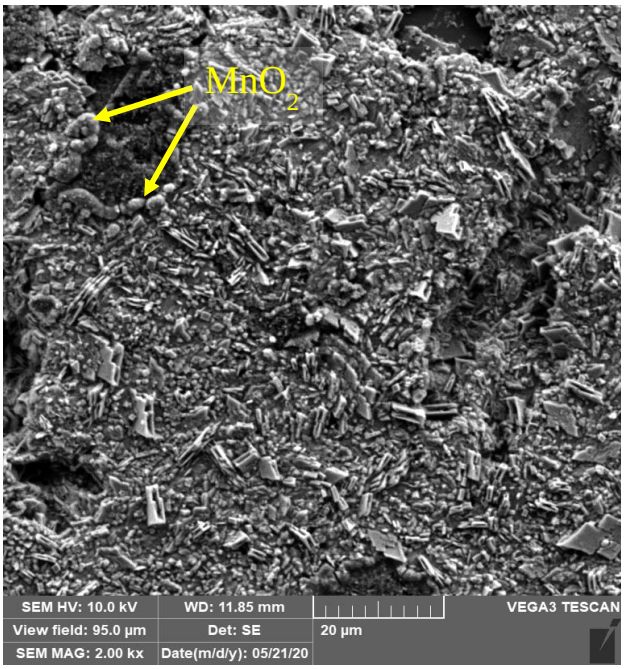

Figure 3.27. SEM micrographs of Pb-Ag anodes after 2 h galvanostatic tests in standard EW solution with 1 g L^{-1} Mn^{2+} at 40 °C.

3.6 Determination of oxide layer and elemental compositions by XRD characterization after galvanostatic test

The XRD analysis was used to identify the different phases and reveal their crystalline structure on the surface of the anodes. After 2 h of galvanostatic test, the surface layer was gently removed from the surface of the anode and collected for XRD analysis. For the fresh anode, the analysis was performed directly on the polished surface of the anode. Figure 3.28 shows the XRD diffractograms for three samples, i.e., fresh anode (a), after galvanostatic test without Mn (b) and with Mn (c). As expected, only the Pb peaks are observed for the fresh anode sample. The surface of the anode in the Mn-free electrolyte is essentially composed of $PbSO_4$, PbO and PbO_2 (Fig. 3.28b). These analyses confirm our interpretation of the results obtained by LSV experiments, stipulating the formation of xPbO.$PbSO_4$ and PbO_2 on the anode surface. Very small amounts of $PbSO_4$ and strong peaks of PbO_2, observed in the pattern (b), suggest that $PbSO_4$ oxidized quickly to PbO_2 when there is no manganese in the solution. The surface of the anode in the electrolyte containing 1 g L^{-1} Mn is essentially composed of MnO_2, $PbSO_4$, PbO and PbO_2 (Fig. 3.28c). In addition to the presence of MnO_2 in this sample, the peaks related to $PbSO_4$ are also much stronger, compared to those observed in pattern (b). This also confirms that, in the presence of Mn, the oxidation of $PbSO_4$ to PbO_2 (reaction 3.1) is suppressed, thus offering a protection against lead oxidation.

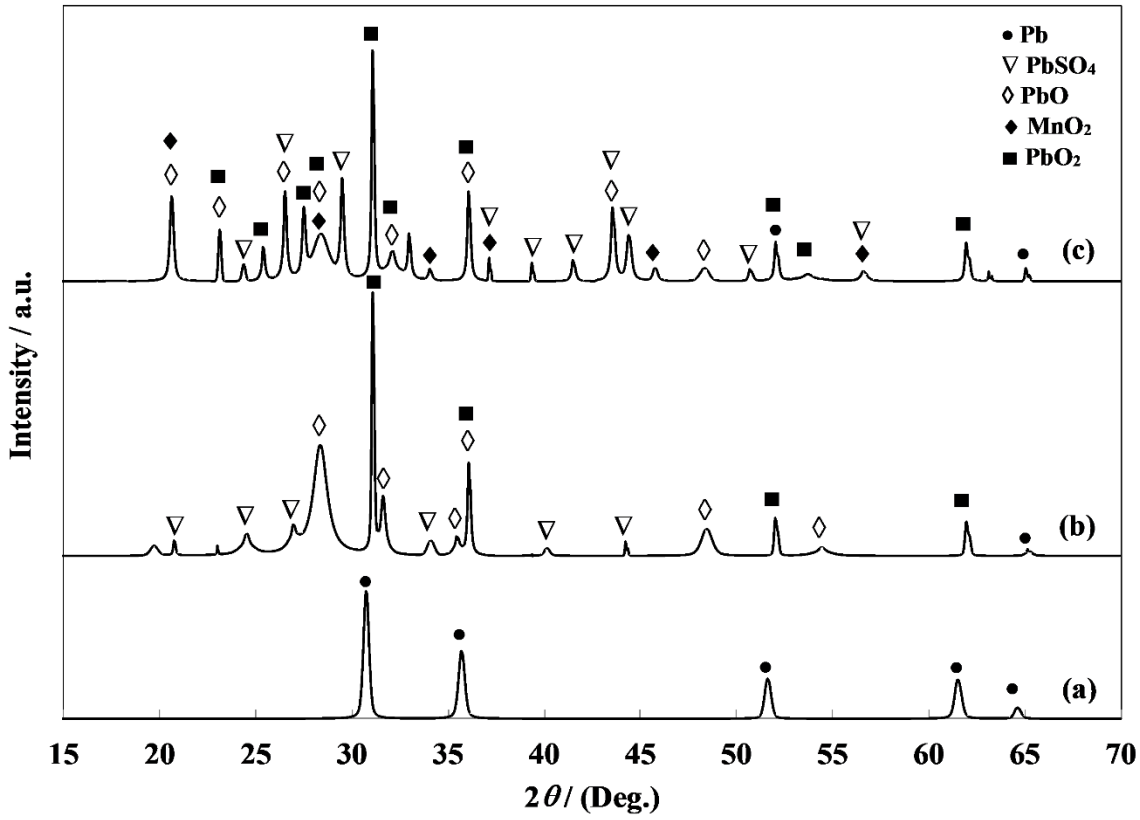

Figure 3.28. XRD patterns of Pb-Ag anodes (a) before galvanostatic test, (b) after 2 h galvanostatic tests without manganese and (c) with 1 g L^{-1} Mn^{2+} at 40 °C.

Conclusion and recommendations for future work

In this work, the optimum operational conditions for obtaining high yield MnO_2 formation on Pb anodes (Pb-0.7wt.%Ag) were investigated in zinc sulfate electrolytes. The concentration of manganese in the electrolyte was measured every 30 minutes by taking a sample from the electrolyte during 2 h of galvanostatic tests and analysing with MP-AES analyser. In order to filter the samples, the filtration with alumina wool was chosen as the best filtration method considering time and cost.

To find the optimum operational conditions, two types of electrolytes were used for simulating the conditions of both electrowinning and purification steps. The galvanostatic tests were performed during 2 h. The electrolyte of electrowinning condition included 55 g L^{-1} Zn^{2+}, 1 g L^{-1} Mn^{2+} at pH 1 while the electrolyte of purification condition included 150 g L^{-1} Zn^{2+}, 1 g L^{-1} Mn^{2+} and pH was adjusted at 4. These tests were carried out by applying various current densities at different temperatures.

In both electrolytes the anodic voltage increased by increasing the current density while the temperature showed adverse effect on the anodic voltage. Moreover, oxygen evolution potential was shifted to the lower values by increasing both temperature and current density. Lower oxygen evolution voltage results in lower manganese deposition on the anode surface, thus decreasing current efficiency of manganese removal. Therefore, for higher current efficiency of manganese removal both temperature and current density must be kept at low values.

For the electrowinning conditions, the highest current efficiency for manganese removal (21 % after 2 h of electrolysis) was obtained for a current density of 125 A m^{-2} at 40 °C. For the purification condition the highest current efficiency, after 2 h of electrowinning, was 2 % at 125 A m^{-2} and same temperature. This suggests that purification electrolyte is not an appropriate environment for manganese removal.

To investigate the effect of pH on current efficiency of manganese removal, we used the electrowinning electrolyte but increased the pH value to 4. A current density of 125 A m^{-2} was applied and the temperature of the electrolyte was kept at 40 °C. This test resulted in a

current efficiency of 4 %, suggesting that the manganese removal is suppressed at higher pH values.

The effect of Mn^{2+} concentrations on anodic current efficiency was also studied in optimal conditions, i.e., at 40 °C at 125 A m^{-2} and pH 1. The results showed very low current efficiency (less than 2 %) when the manganese concentration was 0.1 g L^{-1} and 0.5 g L^{-1}. By increasing manganese concentration from 0.5 g L^{-1} to 1 g L^{-1} the current efficiency increased significantly to 21 %. However, for manganese concentrations between 1 g L^{-1} and 4 g L^{-1} the current efficiency was remained constant.

Cathodic zinc deposition and its current efficiency were also measured in the electrowinning tests. These series of tests conclude that the current efficiency of zinc deposition is increased when the temperature and current density increases. In electrowinning conditions (125 A m^{-2} at 40 °C), a current efficiency of 84 % for zinc deposition was obtained. Moreover, cathodic voltage was decreased when the current density was increased.

Linear sweep voltammetry (LSV) tests were performed and showed that increasing the electrolyte temperature positively affects the oxygen evolution reaction (OER) and depolarizes this reaction. Depolarizing the OER prevents oxidation of manganese and its deposition on the anode. Decreasing the temperature improves the deposition of manganese by preventing oxygen evolution reactions.

Moreover, in the current density vs potential plots generated by LSV, the peak associated with manganese dioxide (MnO_2) increases in intensity by increasing the manganese concentration from 0.1 g L^{-1} to 1 g L^{-1}. In contrast, increasing manganese concentrations from 1 g L^{-1} to 4 g L^{-1} did not alter the intensity of MnO_2 peaks. These results confirm that for manganese concentrations higher than 1 g L^{-1}, current efficiency remained almost constant.

The SEM-EDS characterizations after the galvanostatic tests revealed the presence of MnO_2 layer on the anode. This was accompanied with a sublayer composed of three different phases of MnO_2, PbO_2 and $PbSO_4$. These results were confirmed by performing XRD and XRF analysis.

The results show that, in a best-case scenario, current efficiency of Mn removal is 21 % at a current density of 125 A/m^2. This value is not very high. To enable the proper functioning of MMO anodes, Mn concentration must be decreased to a much lower values, i.e., 100 $mg\ L^{-1}$. With a current efficiency 21 % of and a current density of 125 A/m^2, a great number of anodes would be required to purify the electrolyte, which may not be economically viable. we would therefore suggest increasing the current efficiency of Mn deposition by using other methods. One suggested method may be studying the effect of additives. Alternatively, one can look for other types of anodes exhibiting higher oxygen overpotential, thus suppressing the oxygen evolution reaction.

References

1. Theil, E.C. and K.N. Raymond, *Transition-metal storage, transport, and biomineralization.* Bioinorganic chemistry, 1994: p. 1-35.
2. Weiss, D., T.F. Mason, F. Zhao, G. Kirk, B. Coles and M. Horstwood, *Isotopic discrimination of zinc in higher plants.* New Phytologist, 2005. **165**(3): p. 703-710.
3. Morgan, S., *Zinc and its Alloys and Compounds.* Ellis Horwood, Market Cross House, Cooper Street, Chicester, West Sussex PO 19 1 EB, UK, 1985. 245, 1985.
4. Porter, F.C., *Zinc handbook: properties, processing, and use in design*. 1991: Crc Press.
5. Porter, M.E.P.M., *Competition in global industries*. 1986: Harvard Business Press. 1-76.
6. Sinclair, R.J. *The extractive metallurgy of zinc*. 2005. Australasian Institute of Mining and Metallurgy Victoria.
7. Bratt, G. *A view of zinc electrowinning theory*. in *Tasmania Conference*. 1977.
8. Moats, M.S., *Will lead-based anodes ever be replaced in aqueous electrowinning?* JOM, 2008. **60**(10): p. 46-49.
9. Moats, M., K. Hardee and C. Brown, *Mesh-on-lead anodes for copper electrowinning.* JOM, 2003. **55**(7): p. 46-48.
10. Sandoval, S., R. Garcia, T. Neff and N. Schnebly, *Operation of alternative anodes at Chino SXEW.* Copper 2013 Proceedings Vol. V, 2013.
11. Moats, M.S., *Energy efficiency of electrowinning*, in *Energy Efficiency in the Minerals Industry*. 2018, Springer. p. 213-232.
12. Lee, J.-Y., D.-K. Kang, K. Lee and D. Chang, *An investigation on the electrochemical characteristics of Ta 2 O 5-IrO 2 anodes for the application of electrolysis process.* Materials sciences and applications, 2011. **2**(04): p. 237.
13. Moats, M., *MnO 2 deposition on coated titanium anodes in copper electrowinning solutions.* ERZMETALL, 2010. **63**(6): p. 286-291.
14. Trasatti, S., *Electrocatalysis: understanding the success of DSA®.* Electrochimica Acta, 2000. **45**(15-16): p. 2377-2385.
15. Kayın, P.B., *Removal of cobalt from zinc sulfate solution by cementation prior zinc electrowinning*. 2003. p. 4-8.
16. Rosenqvist, T., *Principles of extractive metallurgy*. 2004: Tapir academic press.
17. Tingle, W., J. Petit and W. Frank, *Handbook of Extractive Metallurgy*. 1997, Edited by F. Habashi, WILEY-VCH, Weinheim, Germany. p. 641-679.
18. Sinclair, R.J. *The extractive metallurgy of zinc*. 2005. Australasian Institute of Mining and Metallurgy Victoria.

19. Nelson, A., W. Wang, G. Demopoulos and G. Houlachi, *The removal of cobalt from zinc electrolyte by cementation: a critical review.* Mineral Procesing and Extractive Metallurgy Review, 2000. **20**(1): p. 325-356.

20. WANG, Y.-f., K.-x. JIANG and H.-b. WANG, *Study on Low Temperature and Pressure Leaching of Marmatite [J].* Nonferrous Metals, 2004. **4**.

21. Xu, Z.-f., Q.-z. Jiang and C.-y. Wang, *Atmospheric oxygen-rich direct leaching behavior of zinc sulphide concentrate.* Transactions of Nonferrous Metals Society of China, 2013. **23**(12): p. 3780-3787.

22. Van der Pas, V. and D. Dreisinger, *A fundamental study of cobalt cementation by zinc dust in the presence of copper and antimony additives.* Hydrometallurgy, 1996. **43**(1-3): p. 187-205.

23. Ferella, F., I. De Michelis and F. Veglio, *Process for the recycling of alkaline and zinc–carbon spent batteries.* Journal of Power Sources, 2008. **183**(2): p. 805-811.

24. Von Röpenack, A., *Future changes in the physico-chemistry of zinc electrowinning.* Lead-Zinc, 1990. **90**: p. 641-652.

25. Buban, K., M. Collins and I. Masters, *Iron control in zinc pressure leach processes.* Jom, 1999. **51**(12): p. 23-25.

26. Sinclair, R.J., *The extractive metallurgy of zinc.* 2005: Australasian Institute of Mining and Metallurgy Victoria.

27. Noubactep, C., *Elemental metals for environmental remediation: Learning from cementation process.* Journal of hazardous materials, 2010. **181**(1-3): p. 1170-1174.

28. Lu, J., D. Dreisinger and K. Rees, *Simultaneous removal of Co, Cu, Cd and Ni from zinc sulfate solution by zinc dust cementation.* Hydrometallurgy, 2020. **197**: p. 105479.

29. Younesi, S., H. Alimadadi, E.K. Alamdari and S. Marashi, *Kinetic mechanisms of cementation of cadmium ions by zinc powder from sulphate solutions.* Hydrometallurgy, 2006. **84**(3-4): p. 155-164.

30. Huang, M., X. Zhou, T. Huang, C. Yang and W. Gui, *Dynamic optimization based on state transition algorithm for copper removal process.* Neural Computing and Applications, 2019. **31**(7): p. 2827-2839.

31. Dib, A. and L. Makhloufi, *Mass transfer correlation of simultaneous removal by cementation of nickel and cobalt from sulfate industrial solution containing copper: Part I: Onto rotating zinc electrode disc.* Chemical Engineering Journal, 2007. **130**(1): p. 39-44.

32. Maja, M. and P. Spinelli, *Detection of metallic impurities in acid zinc plating baths.* Journal of the Electrochemical Society, 1971. **118**(9): p. 1538.

33. Boyanov, B., V. Konareva and N. Kolev, *Removal of cobalt and nickel from zinc sulphate solutions using activated cementation.* Journal of Mining and Metallurgy B: Metallurgy, 2004. **40**(1): p. 41-55.

34. Mureşan, L., G. Maurin, L. Oniciu and D. Gaga, *Influence of metallic impurities on zinc electrowinning from sulphate electrolyte.* Hydrometallurgy, 1996. **43**(1-3): p. 345-354.

35. Fountoulakis, S.G., *Studies on the cementation of cobalt with zinc in the presence of copper and antimony additives.* Diss. Abstr. Int., 1984. **44**(8): p. 289.

36. Tozawa, K., T. Nishimura, M. Akahori and M.A. Malaga, *Comparison between purification processes for zinc leach solutions with arsenic and antimony trioxides.* Hydrometallurgy, 1992. **30**(1-3): p. 445-461.

37. Raghavan, R., P. Mohanan and S. Verma, *Modified zinc sulphate solution purification technique to obtain low levels of cobalt for the zinc electrowinning process.* Hydrometallurgy, 1999. **51**(2): p. 187-206.

38. Hall, D., *Electrodeposited Zinc--Nickel Alloy Coatings--a Review.* Plat. Surf. Finish., 1983. **70**(11): p. 59-65.

39. Loto, C., *Electrodeposition of zinc from acid based solutions: a review and experimental study.* Asian Journal of Applied Sciences, 2012. **5**(6): p. 314-326.

40. Nguyen, T.K.T., *Study Of The Mechanism By Which Cobalt Ions Minimize Corrosion Of Lead Alloy Anodes During Electrowinning Of Base Metals.* 2007.

41. Bratsch, S.G., *Standard electrode potentials and temperature coefficients in water at 298.15 K.* Journal of Physical and Chemical Reference Data, 1989. **18**(1): p. 1-21.

42. Bockris, J.O.M., *Recent developments in the study of hydrogen overpotential.* Chemical reviews, 1948. **43**(3): p. 525-577.

43. Mackinnon, D., J. Brannen and P. Fenn, *Characterization of impurity effects in zinc electrowinning from industrial acid sulphate electrolyte.* Journal of applied electrochemistry, 1987. **17**(6): p. 1129-1143.

44. Fukubayashi, H.H., T.J. O'Keefe and W.C. Clinton, *Effect of Impurities and Additives on the Electrowinning of Zinc*. Vol. 7966. 1974: US Bureau of Mines. 20-25.

45. Neyerlin, K., W. Gu, J. Jorne and H.A. Gasteiger, *Study of the exchange current density for the hydrogen oxidation and evolution reactions.* Journal of The Electrochemical Society, 2007. **154**(7): p. B631.

46. Sinclair, R.J., *The extractive metallurgy of zinc*. 2005: Australasian Institute of Mining and Metallurgy Victoria. 117-121.

47. Peulon, S. and D. Lincot, *Mechanistic study of cathodic electrodeposition of zinc oxide and zinc hydroxychloride films from oxygenated aqueous zinc chloride solutions.* Journal of the Electrochemical Society, 1998. **145**(3): p. 864.

48. Goux, A., T. Pauporté, J. Chivot and D. Lincot, *Temperature effects on ZnO electrodeposition.* Electrochimica Acta, 2005. **50**(11): p. 2239-2248.

49. Scott, A., R. Pitblado, G. Barton and A. Ault, *Experimental determination of the factors affecting zinc electrowinning efficiency.* Journal of applied electrochemistry, 1988. **18**(1): p. 120-127.

50. Cachet, C., C. Le Pape-Rérolle and R. Wiart, *Influence of Co2+ and Mn2+ ions on the kinetics of lead anodes for zinc electrowinning.* Journal of applied electrochemistry, 1999. **29**(7): p. 811-818.

51. Sorour, N., C. Su, E. Ghali and G. Houlachi, *Effect of ionic liquid additives on oxygen evolution reaction and corrosion behavior of Pb-Ag anode in zinc electrowinning.* Electrochimica Acta, 2017. **258**: p. 631-638.

52. James, S., J. Watson and J. Peter, *Zinc production–a survey of existing smelters and refineries.* Lead-Zinc 2000, 2000: p. 203-226.

53. Frausto de Silva, J. and R. Williams, *The biological chemistry of the elements, Chapter: 17.9*. 1991, Dxford.

54. Vereecken, J. and R. Winand, *Influence of manganous ions on the anodic oxidation of methanol.* Electrochimica Acta, 1972. **17**(2): p. 271-278.

55. Hayes, S.A., P. Yu, T.J. O'Keefe, M.J. O'Keefe and J.O. Stoffer, *The Phase Stability of Cerium Species in Aqueous Systems: I. E-pH Diagram for the System.* Journal of the Electrochemical Society, 2002. **149**(12): p. C623.

56. Krupkowa, D., H. Jurczyk, K. Krezel, J. Nosel, A. Gluszczyszyn and M. Mendyka, *Zinc electrowinning.* Pl Patent, 1977(89821).

57. MacKinnon, D. and J. Brannen, *Effect of manganese, magnesium, sodium and potassium sulphates on zinc electrowinning from synthetic acid sulphate electrolytes.* Hydrometallurgy, 1991. **27**(1): p. 99-111.

58. Newnham, R., *Corrosion rates of lead based anodes for zinc electrowinning at high current densities.* Journal of applied electrochemistry, 1992. **22**(2): p. 116-124.

59. Yoshida, T., M. Kahata, M. Dobashi and M. Suzuki, *Chlorine anion elimination from zinc sulphate solution by periodical current reverse electrolytic system.* Aqueous Electrotechnologies: Progress in Theory and Practice, 1997: p. 177-188.

60. Ivanov, I., *Increased current efficiency of zinc electrowinning in the presence of metal impurities by addition of organic inhibitors.* Hydrometallurgy, 2004. **72**(1-2): p. 73-78.

61. Hosny, A., T.J. O'Keefe and W.J. James, *Hull cell technique for evaluating zinc sulfate electrolytes.* Minerals Engineering, 1989. **2**(3): p. 415-423.

62. Ivanov, I. and Y. Stefanov, *Electroextraction of zinc from sulphate electrolytes containing antimony ions and hydroxyethylated-butyne-2-diol-1, 4: Part 3. The influence of manganese ions and a divided cell.* Hydrometallurgy, 2002. **64**(3): p. 181-186.

63. Cathro, K., *Electrowinning zinc at high current density.* 1991.

64. Rerolle, C. and R. Wiart, *Kinetics of oxygen evolution on Pb and Pb-Ag anodes during zinc electrowinning.* Electrochimica acta, 1996. **41**(7-8): p. 1063-1069.

65. Pajunen, L., J. Aromaa and O. Forsén, *The effect of dissolved manganese on anode activity in electrowinning.* Electrometallurgy and Environmental Hydrometallurgy, 2003. **2**: p. 1255-1265.

66. Zhang, W. and C.Y. Cheng, *Manganese metallurgy review. Part II: Manganese separation and recovery from solution.* Hydrometallurgy, 2007. **89**(3-4): p. 160-177.

67. Von Sonntag, C. and U. Von Gunten, *Chemistry of ozone in water and wastewater treatment*. 2012: IWA publishing.

68. Oyama, S.T., *Chemical and catalytic properties of ozone.* Catalysis Reviews, 2000. **42**(3): p. 279-322.

69. Bolton, G.L., V.B. Sefton and N. Zubryckyj, *Removal of manganese and chloride ions from aqueous acidic zinc sulphate solutions*. 1983, Google Patents.

70. Ichlas, Z., M. Mubarok, A. Magnalita, J. Vaughan and A. Sugiarto, *Processing mixed nickel-cobalt hydroxide precipitate by sulfuric acid leaching followed by selective oxidative precipitation of cobalt and manganese.* Hydrometallurgy, 2020. **191**: p. 105185.

71. Langlais, B., D.A. Reckhow and D.R. Brink, *Ozone in water treatment: application and engineering*. 2019: Routledge. 133-138.

72. Zhang, W., P. Singh and D. Muir, *Oxidative precipitation of manganese with SO2/O2 and separation from cobalt and nickel.* Hydrometallurgy, 2002. **63**(2): p. 127-135.

73. Demopoulos, G., L. Rosato and Q. Wang, *Removal of manganese for control of zinc-ore leach flow circuits.* WO Patent, 2001(2001048255).

74. Zhang, W., C.Y. Cheng and Y. Pranolo, *Investigation of methods for removal and recovery of manganese in hydrometallurgical processes.* Hydrometallurgy, 2010. **101**(1-2): p. 58-63.

75. Ferron, C., *Purification of zinc-ore leach solutions by oxidation of manganese impurity.* WO Patent, 2000(2000061826).

76. Pérez-Garibay, R., S. Bello-Teodoro and J.C. Rojas-Montes, *Thermodynamic simulation of the reaction mechanism of Mn2+ oxidation with an SO2/O2 mixture.* Hydrometallurgy, 2018. **176**: p. 260-265.

77. Mulaudzi, N. and T. Mahlangu, *Oxidative precipitation of Mn (II) from cobalt leach solutions using dilute SO2/air gas mixture.* Journal of the Southern African Institute of Mining and Metallurgy, 2009. **109**(6): p. 375-382.

78. PeÌ rez-Garibay, R. and J. Bouchard, *Synthesis of Different Manganese Oxides Using SO2/O2 Gas Mixtures at Different Temperatures.* Industrial & Engineering Chemistry Research, 2014.

79. Mouton, M., J. van Deventer and J. Vaarno. *Oxidative precipitation of Fe and Mn by air/SO2*. in *The Fourth South African Conference on Base Metals. The Southern African Institute of Mining and Metallurgy*. 2007.

80. Burkin, A., G. Manning and A. Monhemius, *Applications of Hydrogen Peroxide and Peroxysulfuric Acids in Hydrometallurgy.* Hydrometallurgy 81, 1981: p. 1981.

81. Burkin, A. and K. Chouzadjian, *Precipitation of manganese dioxide from zinc electrolyte solution using peroxymonosulfuric acid.* Hydrometallurgy Research, Development and Plant Practice, 1983: p. 603-615.

82. Wang, Y. and C. Zhou, *Hydrometallurgical process for recovery of cobalt from zinc plant residue.* Hydrometallurgy, 2002. **63**(3): p. 225-234.

83. Bolton, G.L., V.B. Sefton and N. Zubryckyj, *Removal of manganese ions from zinc and manganese containing solutions*. 1981, Google Patents.

84. Ipinza, J., J. Ibanez, A. Pagliero and F. Vergara, *Formation mechanism of manganese compounds in acidic electrolytes of copper.* Revista de Metalurgia, 2007. **43**(1): p. 11-19.

85. Verbaan, B. and B. Mullinder, *The simultaneous electrowinning of manganese dioxide and zinc from purified neutral zinc sulphate at high current efficiencies.* Hydrometallurgy, 1981. **7**(4): p. 339-352.

86. Zhang, W. and C.Y. Cheng, *Manganese metallurgy review. Part III: Manganese control in zinc and copper electrolytes.* Hydrometallurgy, 2007. **89**(3-4): p. 178-188.

87. Shaw, D. *Iron, chloride and permanganate control in copper electrowinning tankhouses*. in *Proc. COPPER 99 Int. Conf.* 1999.

88. Rodrigues, J. and M. Dry. *The production of particulate manganese dioxide during zinc electrowinning*. in *Proceedings of the International Symposium on Electrometallurigical Plant Practice*. 1990. Elsevier.

89. Ivanov, I., Y. Stefanov, Z. Noncheva, M. Petrova, T. Dobrev, L. Mirkova, R. Vermeersch, and J.-P. Demaerel, *Insoluble anodes used in hydrometallurgy: Part I. Corrosion resistance of lead and lead alloy anodes.* Hydrometallurgy, 2000. **57**(2): p. 109-124.

90. Prengaman, R.D., *The metallurgy of lead alloys for electrowinning anodes.* Anodes for Electrowinning, 1984: p. 49-57.

91. Umetsu, Y., H. Nozaka and K. Tozawa, *Anodic Behaviour of Pb--Ag Alloys in Sulfuric Acid Solution.* J. Min. Metall. Inst. Jpn., 1985. **101**(1168): p. 375-380.

92. Zhang, W., *Performance of lead anodes used for zinc electrowinning and their effects on energy consumption and cathode impurities*. 2010, Université Laval. p. 8.

93. Zamanian, F. and R. Kashanaki, *Microwave Plasma Atomic emission Spectroscopy (MP-AES)*. Iranian Journal of Laboratory Knowledge, 2018. **6**(3): p. 7 - 14.

94. Technologies, A., *Microwave plasma atomic emission spectroscopy (MP-AES)*, A. Technologies, Editor. 2016. p. 4-5.

95. Goldstein, J., *Practical Scanning Electron Microscopy: Electron and Ion Microprobe Analysis*. 2012: Springer US.

96. Minges, M.L. and A.S.M.I.H. Committee, *Electronic Materials Handbook: Packaging*. 1989: Taylor & Francis.

97. Dinnebier, R.E. and S.J. Billinge, *Principles of powder diffraction.* Powder Diffraction: Theory and Practice, 2008: p. 1-19.

98. Smart, L.E. and E.A. Moore, *Solid state chemistry: an introduction*. 2012: CRC press.

99. Beckhoff, B., B. Kanngießer, N. Langhoff, R. Wedell and H. Wolff, *Handbook of Practical X-Ray Fluorescence Analysis*. Vol. Chap. 5. 2007: Springer Berlin Heidelberg.

100. Hrussanova, A., L. Mirkova, T. Dobrev and S. Vasilev, *Influence of temperature and current density on oxygen overpotential and corrosion rate of Pb–Co3O4, Pb–Ca–Sn, and Pb–Sb anodes for copper electrowinning: Part I.* Hydrometallurgy, 2004. **72**(3-4): p. 205-213.

101. Zhang, C., N. Duan, L. Jiang and F. Xu, *The impact mechanism of Mn2+ ions on oxygen evolution reaction in zinc sulfate electrolyte.* Journal of Electroanalytical Chemistry, 2018. **811**: p. 53-61.

102. Yu, P. and T.J. O'Keefe, *Evaluation of lead anode reactions in acid sulfate electrolytes: II. Manganese reactions.* Journal of the Electrochemical Society, 2002. **149**(5): p. A558.

103. Zhang, Q.B. and Y. Hua, *Effect of Mn2+ ions on the electrodeposition of zinc from acidic sulphate solutions.* Hydrometallurgy, 2009. **99**(3-4): p. 249-254.